Article

Trace-Element Geochemistry of Sulfides in Upper Mantle Lherzolite Xenoliths from East Antarctica

Alexandre V. Andronikov *[ID]**, Irina E. Andronikova and Tamara Sidorinova**

Department of Geochemistry and Laboratories, Czech Geological Survey,
Geologicka 6, 15200 Prague, Czech Republic; irina.andronikova@geology.cz (I.E.A.);
tamara.sidorinova@geology.cz (T.S.)
* Correspondence: alexandre.andronikov@geology.cz

Abstract: Sulfides in upper mantle lherzolite xenoliths from Cretaceous alkaline-ultramafic rocks in the Jetty Peninsula (East Antarctica) were studied for their major and trace-element compositions using SEM and LA-ICP-MS applied in situ. Modal abundance of sulfides is the lowest in Cpx-poor lherzolites $\leq$ Spl-Grt lherzolites $<<$ Cpx-rich lherzolites. Most sulfides are either interstitial (i-type) or inclusions in rock-forming minerals (e-type) with minor sulfide phases mostly present in metasomatic veinlets and carbonate-silicate interstitial patches (m-type). The main sulfide assemblage is pentlandite + chalcopyrite $\pm$ pyrrhotite; minor sulfides are polydymite, millerite, violarite, siegenite, and monosulfide solution (mss). Sulfide assemblages in the xenolith matrix are a product of the subsolidus re-equilibration of primary mss at temperatures below $\leq$300 °C. Platinum group elements (PGE) abundances suggest that most e-type sulfides are the residues of melting processes and that the i-type sulfides are crystallization products of sulfide-bearing fluids/liquids. The m-type sulfides might have resulted from low-temperature metasomatism by percolating sulfide-carbonate-silicate fluids/melts. The PGE in sulfide record processes are related to partial melting in mantle and intramantle melt migration. Most other trace elements initially partitioned into interstitial sulfide liquid and later metasomatically re-enriched residual sulfides overprinting their primary signatures. The extent of element partitioning into sulfide liquids depends on P, T, fO_2, and host peridotite composition.

Keywords: sulfides; trace elements; upper mantle xenoliths; East Antarctica; SEM; LA-ICP-MS

---

1. Introduction

Small stock-like Late Jurassic to Early Cretaceous intrusions of alkaline-ultramafic rocks (mostly alkaline picrite and ultramafic lamprophyre) in the Jetty Peninsula (Prince Charles Mountains, East Antarctica; Figure 1) contain abundant xenoliths representing samples of the subcontinental lithospheric mantle (SCLM) beneath the region [1–6]. The studied area is located on the flank of the small rift system which formed at about 650 Ma and lies on the western side of the larger Lambert–Amery rift system, which was active from the Mesozoic period to the Cenozoic period. A detailed description of the geology of the Prince Charles Mountains is given in [4–7]. The upper mantle xenoliths are mostly lherzolite with subordinate harzburgite, dunite and wherlite. Three main groups of lherzolites were identified on the basis of mineral assemblage, textural relationships between the minerals, and mineral composition: (i) clinopyroxene (Cpx)-poor spinel (Spl) lherzolites, (ii) Cpx-rich Spl herzolites, and (iii) Spl-garnet (Grt) lherzolites [3–5]. The East Antarctic SCLM rocks have experienced multiple episodes of infiltration by silicate, carbonate, and minor sulfide melts; this has resulted in partial melting, recrystallization, and the generation of metasomatic minerals such as carbonates and sulfides [5,7–11]. The deepest-sampled upper mantle rocks (Spl-Grt lherzolite) yield ambient temperatures of 1040–1180 °C with pressures up to 24 kbar that correspond to P-T conditions at depths of 75–80 km [2,4,12].

Sulfide minerals are a common accessory phase (<0.1%) in mantle rocks and are typically represented by pentlandite, pyrrhotite, and chalcopyrite [13–16]. Despite their

insignificant abundances, sulfides are important minerals because they likely control the platinum group element (PGE), siderophile, and chalcophile element budget of mantle rocks and determine their behavior during melting [16–18]. Although sulfides in mantle peridotite xenoliths from different localities have been recently studied to trace their crystallization and subsolidus histories ([13,17–27] and others), studies of the trace element composition of sulfides in mantle xenoliths are scarce and are mostly limited to the PGE.
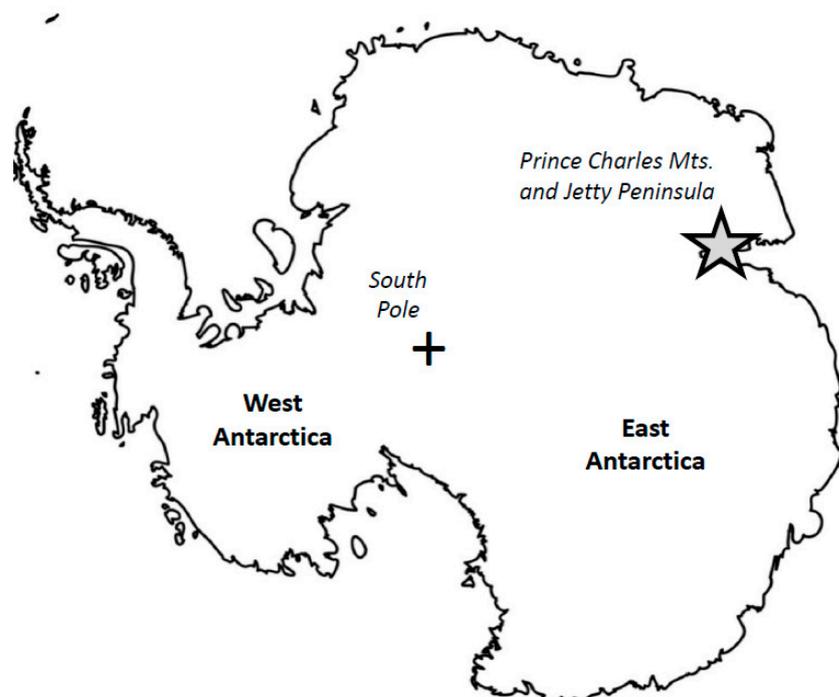

Figure 1. Schematic map of Antarctica showing the position of the Prince Charles Mountains and Jetty Peninsula (asterix).

Sulfide minerals in peridotite xenoliths from East Antarctica were heretofore almost completely unstudied. Only several sulfide grains in Spl-Grt lherzolite xenoliths had been examined via electron microprobe and Raman spectroscopy by Solovova et al. [11]. In order to retrieve information on the origin and evolution of sulfides in mantle xenoliths, we conducted detailed in situ scanning electron microscopy (SEM) and laser ablation inductively coupled plasma mass spectrometric (LA-ICP-MS) analyses of the sulfide phases in SCLM peridotite xenoliths samples from the Jetty Peninsula area. The present work is based on lherzolite xenoliths that have been previously studied in detail for bulk rock and rock-forming mineral geochemistry [2–4,12].

2. Materials and Methods

2.1. Brief Characteristics of Lherzolite Xenoliths

Upper mantle xenoliths in the Jetty Peninsula area are hosted by alkaline ultramafic magmatic rocks (150 $\pm$ 5 Ma) that originated from the melting of the mantle at depths of 120–150 km [1,28,29]. The xenoliths were trapped by ascending magma at depths from 75–80 km up to the crustal–mantle boundary and were rapidly delivered to the surface [4]. The studied lherzolite xenolith samples were collected by the authors from a single magmatic body composed of alkaline picrite.

The Cpx-poor Spl lherzolites are medium to coarse-grained inequigranular rocks composed of 78–82% olivine (Ol), 10–14% orthopyroxene (Opx), 4–7% Cpx, and 1.5–5% Spl. Low concentrations of CaO and Al_2O_3 (0.8–1.5 wt% and 0.5–1.6 wt%, respectively) and a high Mg# (100Mg/(Mg + Fe)) of 90.2 to 91.2 suggesting depletion by partial melting, are characteristic of the rock [3,4]. The history of both significant depletion and later slight

metasomatic enrichment are also confirmed by their U-shaped rare earth element (REE) patterns in CI chondrite-normalized diagrams (see Andronikov [3], Foley et al. [4,5]).

The Cpx-rich Spl lherzolites consist of 66–75% Ol, 11–16% Opx, 9–14% Cpx, and 1–4% Spl. Clinopyroxene and Spl display recrystallized edges resulting from a few episodes of melt infiltration [4,8]. These recrystallized edges contain melt pockets produced either by mineral melting or by melt percolation along the grain boundaries [4,8]. Although the rock is much less depleted than the Cpx-poor lherzolite (Mg# 86.8–90.9; CaO 2.0–3.3 wt%; Al_2O_3 2.2–3.0 wt%), it shows history of both depletion and later metasomatic enrichment [3–5].

The Spl-Grt lherzolites consist of 57–66% Ol, 18–23% Opx, 11–16% Cpx, 2–7% Grt, and 0.2–0.5% Spl. The bulk rock composition is characterized by a Mg# of 89.0–91.2, CaO of 2.3–3.4 wt%, and Al_2O_3 of 2.3–4.1 wt%. Most grains of the original Grt are completely replaced by kelyphite (Kel). The presence of garnet suggests that the xenoliths came from deeper parts of the SCLM (75–80 km) than the Cpx-rich Spl lherzolites, but nevertheless, they experienced similar metasomatic overprints [4].

Chemical compositions of the rock-forming minerals have been previously described in detail in [2–4]. Overall, Ol in the Cpx-poor Spl lherzolites is uniform in composition. Olivine and Opx are Mg-rich (Mg# 90.7–91.4), and Opx displays low Al_2O_3 content (2.4–3.8 wt%). Clinopyroxene-poor Spl lherzolites have only one generation of Cpx, whereas the Cpx-rich Spl lherzolites have two Cpx generations. First generation clinopyroxene is compositionally similar to that in Cpx-poor rocks, whereas second generation Cpx is richer in Fe. Garnet is pyrope-rich (Mg# 82.1–86.8) and contains 1.1–2.0 wt% Cr_2O_3. CaO contents in Grt vary from 1.3 to 5.6 wt%. Spinel displays the highest Cr# (100Cr/(Cr + Al)) in the Cpx-poor Spl lherzolites (26–35) and the lowest in the Spl-Grt lherzolites (14–23), which is consistent with the higher degree of depletion in the Cpx-poor Spl lherzolites.

The Jetty Peninsula xenoliths contain evidence of several stages of enrichment of the SCLM rocks through melts and fluids [4,10,12]. Presence of silicate melts is evidenced by glass composition ranging from sodic basaltic melts to K-rich phonolitic melts along the grain boundaries and as interstitial patches [4,8]. Evidence of immiscible carbonate and sulfide liquids in the mantle rocks is preserved by carbonate-sulfide inclusions in silicate minerals [4] and by CO_2-rich fluid inclusions in the silicate minerals that are described in detail in [10,11]. Multiple events of partial melting and melt extraction events followed by metasomatic re-enrichment in the East Antarctic SCLM may be related to rifting during the breakup of Gondwanaland [4–7].

Thermometry on studied Jetty Peninsula SCLM xenoliths indicates equilibration temperatures ranging from 1100–1135 °C for Spl-Grt lherzolites, to 1090–1100 °C for Cpx-rich Spl lherzolites, and to 850–1035 °C for Cpx-poor Spl lherzolites [4]. Oxygen fugacity (fO_2) relative to the FMQ buffer (Δlog(FMQ)) lies between −0.17 and −2.62 (mean −1.03) for Cpx-poor Spl lherzolites, between +0.15 and −2.13 (mean −0.35) for Cpx-rich Spl lherzolites, and between −0.22 and −1.18 (mean −0.75) for Spl-Grt lherzolites [4,30].

The eight selected xenolith samples vary from the Cpx-poor Spl lherzolites (U-3/4-2, U-1/4-3, 32601-9b) to the Cpx-rich Spl lherzolites (UN-1, XLT-4) and to the Spl-Grt lherzolites (DK-8/3, DN-1, DN-4). This set of xenoliths represents a rock series ranging from almost unmetasomatized and strongly depleted peridotites to peridotites that experienced significant metasomatic re-enrichment.

2.2. Analytical Techniques

Polished rock sample mounts 25 mm in diameter were prepared from the xenolith chips for microscopic study and further SEM and LA-ICP-MS analyses. Sulfide phases were first identified and studied visually using a Carl Zeiss MicroImaging GmbH reflected light microscope equipped with the Axio Imager 2. This microscope was also used for reflected light photomicrographs. Sulfides were then analyzed for major and trace-element concentrations using the SEM and LA-ICP-MS methods. Analyses were conducted by the authors at the Department of Geochemistry and Laboratories of the Czech Geological Survey (Prague, Czech Republic) in 2021.

2.2.1. SEM

The SEM analyses allowed the selection of grains for the LA-ICP-MS runs and to provide the necessary major-element concentrations for quantitative sulfide analysis. Major elements were analyzed using a Tescan MIRA3 GMU FEG-SEM equipped with a wavelength-dispersive spectroscopic microanalyzer (Oxford Instruments Wave, Abingdon, UK). The analyses were conducted with an accelerating voltage of 15 kV, a beam current of 8 nA, and a working distance of 15 mm. Counting times were 20 s at peak position and 10 s at the background positions. Routine sulfide analyses included Fe, Co, Ni, Cu, Zn, and S. For quantitative analyses, the following standards were used: galenite (for S), pyrite (Fe), chalcopyrite (Cu), sphalerite (Zn), pentlandite (Ni), and pure Co (Co). Analyses were processed using INCA software (Oxford Instruments).

2.2.2. LA-ICP-MS

The LA-ICP-MS analytical system consisted of an Agilent 7900 quadrupole (Q)-ICP-MS (Agilent Technologies Inc., Santa Clara, CA, USA) coupled with the Analyte Excite Excimer 193 nm LA system (Photon Machines, Redmond, WA, USA) equipped with a two-volume HelEx ablation cell. The laser gas system included nitrogen for the purging of the laser beam path, helium carrier gas, internal premix argon-fluoride, and flush helium gas. The Q-ICP-MS was equipped with a standard Ni sampler and skimmer cones and a quartz torch with a 2.5 mm glass injector. The laser beam diameter ("spot size") was 12–20 μm (depending on the analyzed sulfide size). The applied laser fluence was 2.83–3.14 J/cm^2 with a laser pulse rate of 10 Hz. A typical analysis consisted of 20 s of background acquisition (gas blank), 30–35 s of sample ablation, and 30–40 s of wash-out time (Figure 2). The GLITTER 3.0 software package was used for data reduction [31,32]. The internal standardization was based on Fe concentrations determined by the SEM analysis and on the stoichiometric Fe values. Two reference materials were used for external calibration: a USGS MASS-1 standard (Fe-Cu-Zn-S pressed powder pellet; [33]) to calibrate Cr, Ni, Ga, Ge, As, Se, Mo, Cd, Ag, Sn, Sb, Te, Au, Pb, and Bi and a UQAC-FeS-1 synthetic versatile reference material from the LabMaTer (University of Quebec in Chicoutimi, Canada; [34–36]) to calibrate Ti, Mn, Co, Cu, Zn, and the PGE. All standards were analyzed at the beginning and at the end of each analytical session in order to monitor the sensitivity drift. A total of 29 isotopes were monitored during the analyses (^{47}Ti, ^{53}Cr, ^{55}Mn, ^{57}Fe, ^{59}Co, ^{61}Ni, ^{65}Cu, ^{66}Zn, ^{71}Ga, ^{74}Ge, ^{75}As, ^{77}Se, ^{95}Mo, ^{99}Ru, ^{103}Rh, ^{107}Ag, ^{108}Pd ^{111}Cd, ^{115}In, ^{118}Sn, ^{121}Sb, ^{125}Te, ^{185}Re, ^{188}Os, ^{193}Ir and ^{195}Pt ^{197}Au, ^{208}Pb, and ^{209}Bi). Element concentrations were calculated using the obtained isotope signal intensities.

A significant problem during routine LA-ICP-MS analysis is the occurrence of interferences. The plasma gas-related polyatomic interferences caused by argides are particularly problematic for the PGE analyses of sulfides containing Ni, Co, Zn or Cu (e.g., ^{99}Ru interferes with ^{59}Co^{40}Ar and ^{63}Cu^{36}Ar; ^{101}Ru with ^{61}Ni^{40}Ar, ^{63}Cu^{38}Ar, and ^{65}Cu^{36}Ar; ^{103}Rh with ^{63}Cu^{40}Ar, ^{65}Zn^{38}Ar, and ^{67}Zn^{36}Ar; ^{105}Pd with ^{65}Cu^{40}Ar; ^{108}Pd with ^{68}Zn^{40}Ar). Isobaric interferences are caused by elements that have the same isotopic masses (e.g., ^{108}Pd with ^{108}Cd, ^{115}In with ^{115}Sn). Some interferences can be avoided or significantly reduced with proper isotope selection. For instance, ^{65}Cu should be measured instead of ^{63}Cu, ^{99}Ru instead of ^{101}Ru, and ^{108}Pd instead of ^{105}Pd; ^{111}Cd instead of ^{108}Cd, ^{118}Sn instead of ^{115}Sn, ^{193}Ir instead of ^{191}Ir, and ^{195}Pt instead of ^{194}Pt. The interference between ^{56}Fe, the main Fe isotope, and ^{40}Ar^{16}O can be avoided by using the minor iron isotope ^{57}Fe [37–39]. Another way to avoid/reduce the influence of these interferences is to use matrix-matched standards while analyzing natural samples.

Because of LA method limitations, the majority of the analyses were conducted on sulfide phases smaller than the interaction volume of the ablation causing beam overlaps between different sulfide phases. Subsurface inclusions were also occasionally encountered during ablation. Nevertheless, we were able to analyze homogeneous sulfide phases in a few cases.
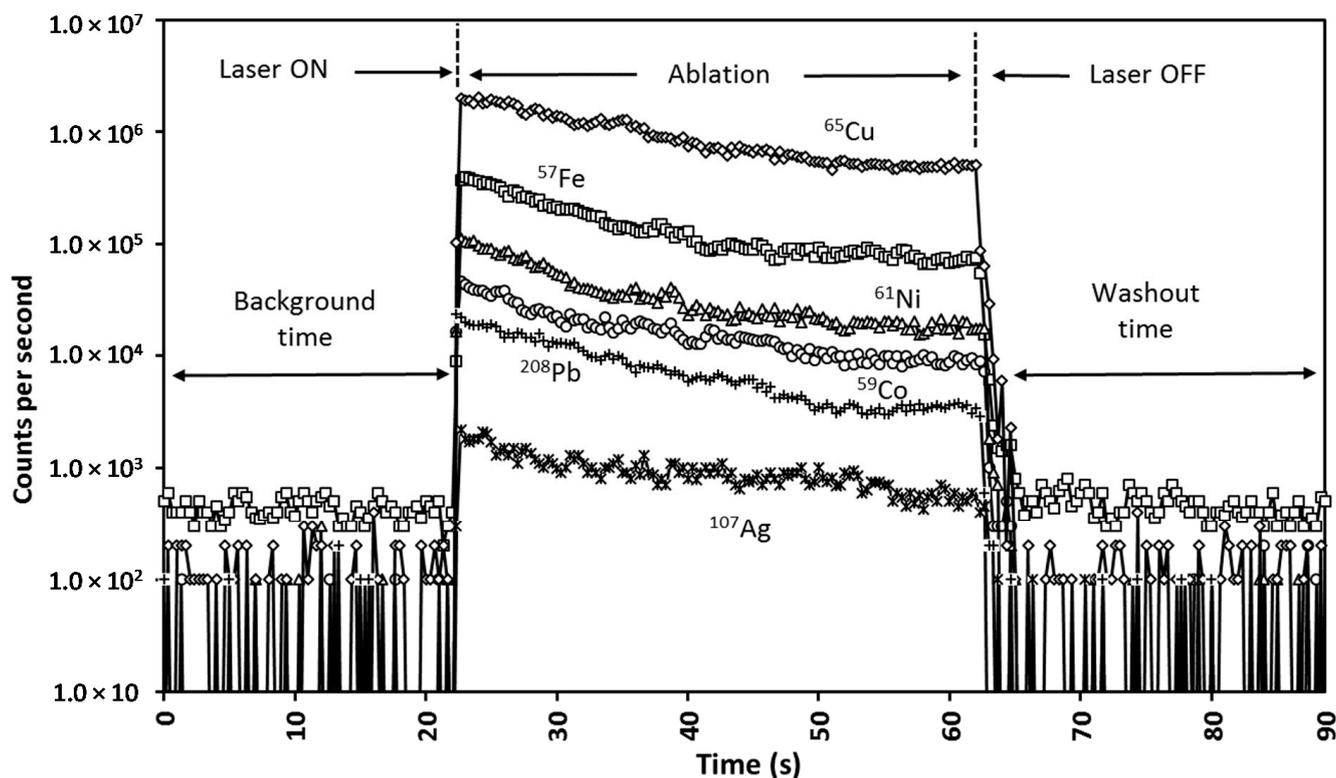
Figure 2. Representative time-resolved LA-ICP-MS depth profiles for sulfides with a few selected isotopes shown (chalcopyrite (Ccp)-bearing pentlandite (Pn) from interstitial sulfide in the Cpx-poor Spl lerzolite sample U-1/4-3; beam diameter is 20 μm). From the left, the background count is 23 s, followed by 42 s of ablation time (which is integrated) and by 40 s of wash-out time (not shown completely).

3. Results

3.1. Sulfide Petrography and Major-Element Composition

Sulfides in the Jetty Peninsula xenoliths occur mostly as interstitial grains and as globular inclusions in silicate minerals and spinel. Less frequent sulfides are present in secondary metasomatic veinlets and in silicate-carbonate patches. We grouped the sulfides into three types according to their textural occurrence (see Westner et al. [27]): sulfides enclosed in silicate minerals and spinel (e-type) occurring as spherical droplet-like grains (although some crystals are sub- to euhedral); interstitial sulfides observed along the grain boundaries of the primary mineral assemblages appearing as droplet-like, irregular, or blocky grains (i-type); and sulfides associated with metasomatic veinlets and silicate-carbonate patches (m-type). Modal abundance of sulfide minerals in the studied xenoliths is as follows: Cpx-poor lherzolites ≤ Spl-Grt lherzolites << Cpx-rich lherzolites. Major-element characteristics of the studied sulfides are given in Tables 1–4.

Table 1. Representative SEM analyses of sulfides in Cpx-poor Spl lherzolites from East Antarctica (wt%).

	Inter				In Ol						
Sample	U-3/4-2				U-1/3-4						
Mineral	**Pn**	**Pn**	**Ccp**	**Ccp**	**Pn**	**Pn**	**Pn**	**Ccp**	**Ccp**	**Pld**	**Pld**
Zn		0.08		0.02				0.01			
Cu	0.44	0.12	30.64	30.29	0.29	0.62	0.18	31.47	32.51	0.56	0.09
Ni	37.98	36.48	0.38	0.09	42.97	43.18	43.36	2.36	0.76	49.76	52.20
Co		0.38	0.01	0.01	0.39	0.40	0.32	0.02	0.08	0.79	0.54
Fe	25.56	25.76	28.31	29.62	22.36	22.30	21.95	28.77	29.71	6.45	3.04
S	32.34	31.00	33.70	34.29	32.65	32.95	32.67	33.97	34.32	39.23	41.01
Total	96.32	93.82	93.04	94.33	98.67	99.45	98.48	96.60	97.38	96.79	96.88

	Inter											
Sample	32601-9b								U-1/3-4			
Mineral	**Ccp**	**Ccp**	**Pld**	**Pld**	**Pld**	**Pn**	**Pn**	**Pld**	**Ccp**	**Cu-Ni ss**	**Cu-Ni ss**	**Cu-Ni ss**
Zn	0.05	0.13					0.08		0.16	0.07		
Cu	33.09	30.79	0.50	0.62	0.38	0.18	0.23	0.15	31.75	13.09	22.04	7.58
Ni	0.47	1.21	54.18	53.25	53.78	37.77	37.80	49.17	1.06	44.93	38.11	48.03
Co	0.05	0.19	1.25	1.92	1.69	0.26	0.46	0.39	0.01	0.54	0.18	0.89
Fe	30.05	27.52	1.20	1.71	1.31	26.26	26.48	5.62	29.55	1.06	1.18	0.95
S	34.92	34.06	41.91	42.49	42.35	32.47	32.56	40.70	34.50	37.80	36.29	39.37
Total	98.63	93.90	99.04	99.99	99.51	96.94	97.61	96.03	97.03	97.49	97.80	96.82

Inter, interstitial; Ol, olivine; Pn, pentlandite; Ccp, chalcopyrite; Pld, polydymite; Cu-Ni ss, Cu-Ni monosulfide solution.

Table 2. Representative SEM analyses of sulfides in Cpx-rich Spl lherzolites from East Antarctica (wt%).

	In Ol					In Spl					
Sample	UN-1										
Mineral	**Po**	**Po**	**Pn**	**Pn**	**Ccp**	**Po**	**Pn**	**Pn**	**Ccp**	**Ccp**	**mss**
Zn		0.09			0.31		0.21		0.01	0.14	
Cu	0.16	0.06	0.13	0.08	32.47	0.09			33.30	33.52	2.92
Ni	0.94	1.14	35.18	33.78	0.52	2.27	37.52	35.42	0.36	0.27	20.28
Co		0.07	0.45		0.09		0.62	0.66	0.08	0.04	0.22
Fe	54.54	54.69	27.78	27.68	28.18	51.86	25.74	27.69	28.61	28.57	31.41
S	38.96	37.51	31.48	31.70	32.28	39.28	31.07	30.47	32.82	32.81	33.44
Total	94.60	93.56	95.02	93.24	93.85	93.50	95.16	94.24	95.18	95.35	88.27

	Inter										
Sample	UN-1						XLT-4				
Mineral	**Po**	**Po**	**Pn**	**Pn**	**Ccp**	**Ccp**	**Pn**	**Pn**	**Ccp**	**Ccp**	**Mlr?**
Zn					0.07						
Cu	0.15	0.04			31.98	32.38	0.82	0.53	34.12	33.14	0.39
Ni	0.54	0.40	37.55	38.36	0.33	0.45	41.62	40.89	0.47	0.64	52.22
Co	0.15	0.11	0.63	0.55		0.01	0.55				
Fe	57.48	56.68	26.73	26.36	29.28	29.11	21.44	24.62	29.87	30.16	11.19
S	39.33	39.10	32.48	32.84	34.76	34.02	32.35	33.55	34.80	35.09	34.38
Total	97.65	96.33	97.39	98.11	96.42	95.97	96.78	99.59	99.26	99.03	98.18

	In Ol							
Sample	XLT-4							
Mineral	**Pn**	**Pn**	**Ccp**	**Ccp**	**mss**	**mss**	**Mlr**	**Mlr**
Zn								
Cu	0.38	0.37	34.36	33.25	1.14	1.44	0.46	0.06
Ni	39.72	39.35	0.11	0.51	34.16	30.47	57.17	58.60
Co					0.63	0.63		
Fe	24.23	24.85	29.17	28.82	15.48	19.19	6.00	3.54
S	33.56	33.66	34.23	34.22	35.19	35.64	34.95	35.30
Total	97.89	98.23	97.87	96.80	86.60	87.37	98.58	97.50

Spl, spinel; mss, monosulfide solution; Po, pyrrhotite; Mlr, millerite.

Table 3. Representative SEM analyses of sulfides in Spl-Grt lherzolites from East Antarctica (wt%).

	Inter							In Ol		
Sample	DK-8/3							DN-4		
Mineral	Pn	Ccp	Ccp	Ccp	Fe-Mlr	Fe-Mlr	Fe-Mlr	Pn	Ccp	Pld
Zn		0.12	0.03						0.01	
Cu	1.14	33.32	33.31	33.25	0.63	0.68	0.34	0.20	32.83	
Ni	39.85	0.33	0.45	0.84	60.55	62.00	62.61	42.08	0.28	50.51
Co	0.53		0.08	0.07	0.80	0.52	0.25	0.37		0.42
Fe	23.12	30.28	30.58	30.99	3.31	2.39	2.95	23.77	29.40	7.99
S	32.93	32.75	31.69	31.91	32.87	32.21	31.75	31.65	33.79	38.60
Total	97.57	96.80	96.14	97.06	98.16	97.80	97.90	98.07	96.31	97.52

	In kelyphite					
Sample	DN-1					
Mineral	Po	Po	Pn	Pn	Ccp	Ccp
Zn			0.05		0.04	
Cu	0.06			0.06	33.62	33.29
Ni	1.89	1.18	41.18	38.24	0.60	0.50
Co	0.03	0.05	0.35	0.26	0.04	0.13
Fe	58.58	58.41	24.46	28.26	31.50	29.94
S	35.73	36.06	29.69	29.27	32.15	31.69
Total	96.29	95.70	95.73	96.09	97.95	95.55

Table 4. SEM analyses of m-type sulfides in lherzolites from East Antarctica (wt%).

Rock	Cpx-poor			Spl-Grt						
Type	Skeletal									
Loation	Veinlet									
Sample	32601-9b			DN-4						
Mineral	Co-Mlr	Sgn	Sgn	Co-Vo	Co-Vo	Co-Vo	Co-Mlr	Co-Mlr	Co-Mlr	Co-Mlr
Zn			0.04							
Cu							0.08			0.01
Ni	60.05	44.14	36.68	53.29	53.24	45.08	60.38	59.21	58.93	61.79
Co	2.47	11.36	17.09	2.15	1.75	8.61	1.85	2.04	3.16	0.96
Fe	0.04	0.31	0.98	1.09	1.10	2.74	1.23	1.32	1.43	1.13
S	33.13	42.04	41.19	40.58	40.72	40.77	34.07	33.99	33.73	34.01
Total	95.69	97.85	95.98	97.11	96.81	97.20	97.61	96.56	97.25	97.90

Rock	Spl-Grt								
Type	Massive							Faceted	
Location	Patch							Patch	
Sample	DN-4							DN-4	
Mineral	Py	Py	Py	Py	Py	Py	Py	Py	Py
Zn	0.16		0.04		0.15	0.06			0.02
Cu	0.10					0.05			
Ni	0.05		0.07			0.06	0.03	0.39	0.04
Co	0.12	0.03	0.04	0.07	0.09	0.05	0.09	0.05	0.01
Fe	45.25	45.87	45.22	45.41	45.25	45.14	45.15	41.18	42.99
S	49.96	48.93	49.67	49.15	48.85	49.24	49.16	43.88	43.26
Total	95.64	94.83	95.04	94.63	94.34	94.60	94.43	85.50	86.32

Cpx, clinopyroxene; Spl, spinel; Grt, garnet; Sgn, siegenite; Co-Vo, Co-violarite; Py, pyrite.

3.1.1. Sulfides in Cpx-Poor Spl Lherzolites

Sulfides occur as very rare inclusions (40–100 μm size) in primary minerals and as irregular to oval interstitial grains of 2 to 70 μm in size between silcate minerals (Figure 3a–e). A separate type of sulfides is mostly represented by two-phase irregular or elongated grains of 20–50 μm size (Figure 3f) and by rare skeletal crystals of about 10 × 25 μm in size in metasomatic veinlets cross-cutting primary minerals (Figure 3g).

Sulfide inclusions in primary minerals are represented by two major phases: pentlandite (34–40 wt% Ni, 22–28 wt% Fe, 0–0.4 wt% Pb) and chalcopyrite (32–34 wt% Cu, 27–29 wt% Fe, 0.1–0.5 wt% Ni). Chalcopyrite is developed along the cleavage cracks and/or as massive blebs inside the pentlandite matrix. Commonly fractured pyrrhotite is developed in marginal parts of the sulfide inclusions (Figure 3a). Additionally, secondary polydymite (50–52 wt% Ni, 3.0–6.5 wt% Fe) can be developed along the sulfide bleb edges (Figure 3a). Three- and two-phase interstitial sulfides are represented by pentlandite (36–38 wt% Ni, 25–26 wt% Fe, 0.1–0.4 wt% Cu), chalcopyrite (29–31 wt% Cu, 28–29 wt.% Fe), and, in the case of three-phase sulfides, polydymite (50–54 wt% Ni, 1.2–5.6 wt% Fe) (Figure 3c,d). In large interstitial sulfides, slightly cleaved pentlandite forms the main volume of the sulfide. Chalcopyrite is developed along cleavage cracks in pentlandite and as an outer rim of the pentlandite body. Spongy interstitial sulfide observed in triple points between silicate minerals (Figure 3e) is represented by Ni-Cu mss (1.0–3.8 wt% Fe, 6–22 wt% Cu, 38–48 wt% Ni). Tiny Ti oxides and bornite are developed around the Cu-Ni mss. Sulfides in metasomatic veinlets (Figure 3f,g) are represented by two-phase crystals consisting of massive chalcopyrite (31–33 wt% Cu, 28–30 wt% Fe, 0.5–1.2 wt% Ni) and polydymite (53–54 wt% Ni, 1.2–3.2 wt% Fe, 1.0–1.9 wt% Co) as well as by two-phase skeletal crystals composed of siegenite (37–44 wt% Ni, 0.3–1.0 wt% Fe, 11–17 wt% Co) and Co-millerite (60 wt% Ni, 2.5 wt% Co).

3.1.2. Sulfides in Cpx-Rich Spl Lherzolites

Here, sulfides occur as globular inclusions (e-type sulfides) of 1 to 150 μm in size in silicate minerals and spinel (Figure 4a–c) and as irregular interstitial grains of 5 to 350 μm in size (Figure 4d–f). Larger sulfide inclusions can be accompanied by chains/tails of very small inclusions (1–3 μm) that are commonly located along the existing and/or healed cracks in the host mineral (Figure 4b,c). Compositionally, sulfide inclusions in silicate minerals are represented by three major phases: pentlandite (34–40 wt% Ni, 22–28 wt% Fe), pyrrhotite (52–56 wt% Fe, 0.3–2.3 wt% Ni), and chalcopyrite (32–34 wt% Cu, 27–29 wt% Fe, 0.1–0.5 wt% Ni). Inclusions in spinel are represented by pentlandite (33–38 wt% Ni, 26–28 wt% Fe) and chalcopyrite (31–32 wt% Cu, 27–28 wt% Fe). A monosulfide solution characterized by high amounts of Ni (20.3–34.2 wt%) at slightly lower amounts of Fe (15.5–31.4 wt%) was found in the lateral parts of the sulfide inclusions (Figure 4a,c). Most interstitial (i-type) sulfides in Cpx-rich Spl lherzolites are represented by two-, or rarely, three-phase grains. Three-phase interstitial sulfides occur as very big blocky grains (150–350 μm) characterized by flame-like occurrences of pentlandite (37–38 wt% Ni, 26–27 wt% Fe) inside massive pyrrhotite (56–57 wt% Fe, 0.4–0.5 wt% Ni) (Figure 4d). Chalcopyrite (31–32 wt% Cu, 28–29 wt% Fe) can be developed along the edges of the grain and inside the dominant pyrrhotite + pentlandite assemblage, and/or as exsolution lamellae along the cleavage cracks in pentlandite. Two-phase sulfides are usually composed of cleaved pentlandite (35–41 wt% Ni, 23–27 wt% Fe) in the core part of sulfide blebs and chalcopyrite (30–33 wt% Cu, 28–29 wt% Fe, 0.2–0.9 wt% Ni) that has developed either at the massive phase at the edges and in the center of sulfide grain or as fine exsolution lamellae along the cleavage cracks in pentlandite (Figure 4e,f). Iron oxides can be developed along the outer oxidized parts of sulfide grains (Figure 4e). Iron-bearing millerite (52–59 wt% Ni, 4–11 wt% Fe) was identified in marginal parts of some pentlandite-rich interstitial sulfide showing mss break up structures (Figure 4f). High-Fe millerite (11 wt% Fe) is, in reality, likely a mixture of mostly millerite with an insignificant amount of pentlandite.
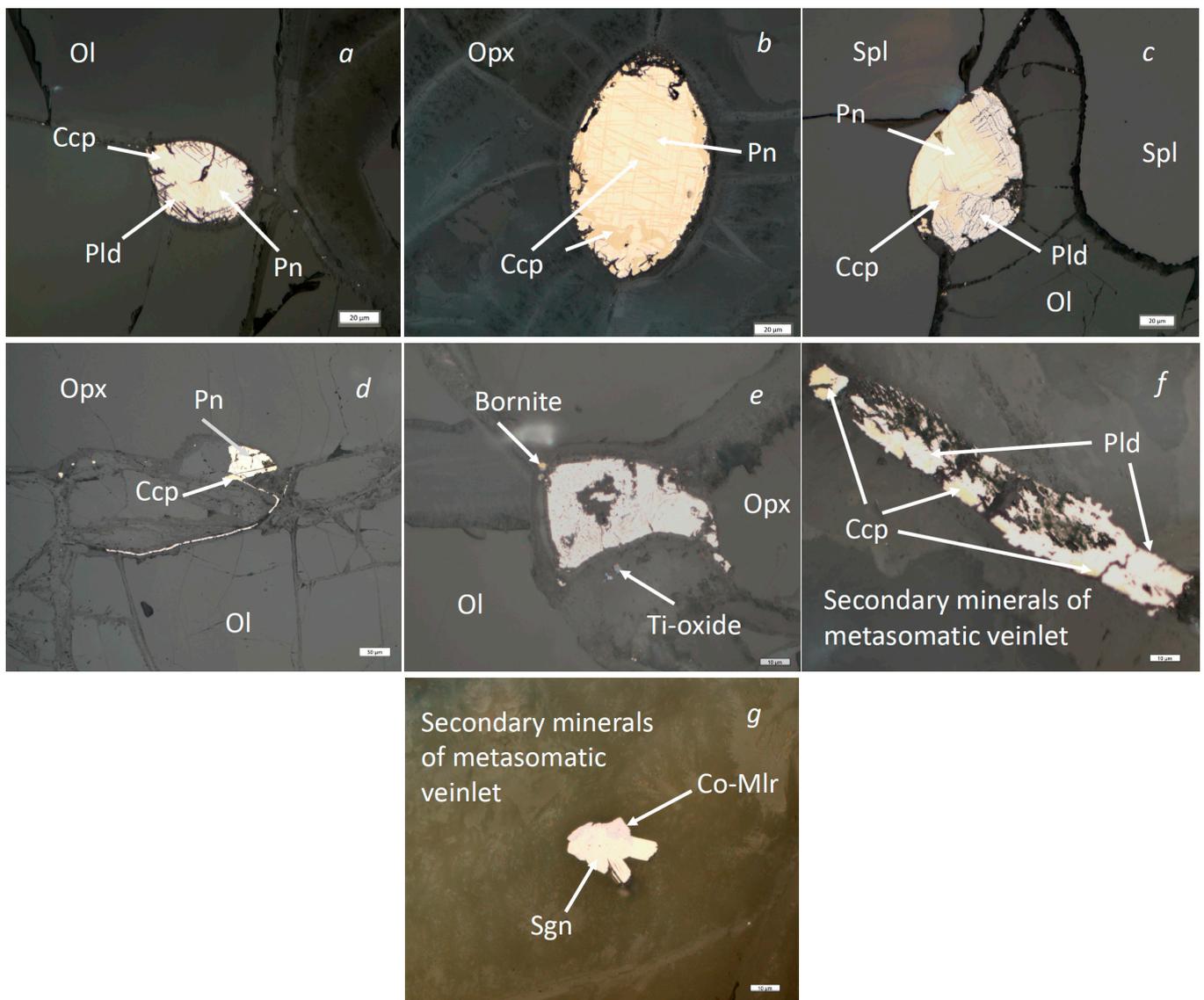
Figure 3. Reflected light photomicrographs of sulfide structural types from Cpx-poor Spl lherzolites: (**a**) multi-phase oval sulfide inclusion (e-type sulfide) in Ol. The main body consists of Pn with Ccp forming lamellae along the cleavage cracks; insignificant volume at the marginal part of the inclusion is occupied by Ccp. Cleaved polydymite (Pld) has developed along the edges of the inclusion; the scale bar is 20 μm; (**b**) bi-mineralic Pn + Ccp sulfide inclusion (e-type sulfide) in Opx. The main body consists of Pn with Ccp forming lamellae along the cleavage cracks. Massive Ccp is developed at marginal parts of the inclusion. The scale bar is 20 μm; (**c**) i-type interstitial multi-phase oval sulfide. The main body consists of Pn with Ccp forming lamellae along the cleavage cracks. mss is sporadically developed at the very edge of the sulfide bleb. Cleaved/cracked Pld is developed along the edges of the sulfide bleb, The scale bar is 20 μm; (**d**) irregular interstitial (i-type) bi-mineral Pn + Ccp sulfide complicated by the bi-mineralic (Pn + Ccp) sulfide film along the silicate grain boundaries. The scale bar is 50 μm; (**e**) interstitial spongy Cu-Ni mss. Bornite and Ti-oxide crystals are developed around the mss. Tiny Fe-oxide crystals are developed within the main body of the mss. The scale bar is 10 μm; (**f**) elongated bi-mineral Pn + Ccp sulfide of m-type in a metasomatic veinlet. The scale bar e is 10 μm; (**g**) skeletal siegenite (Sgn) + Co-milerite (Mlr) crystal (m-type sulfide) in a metasomatic veinlet. The scale bar is 10 μm.
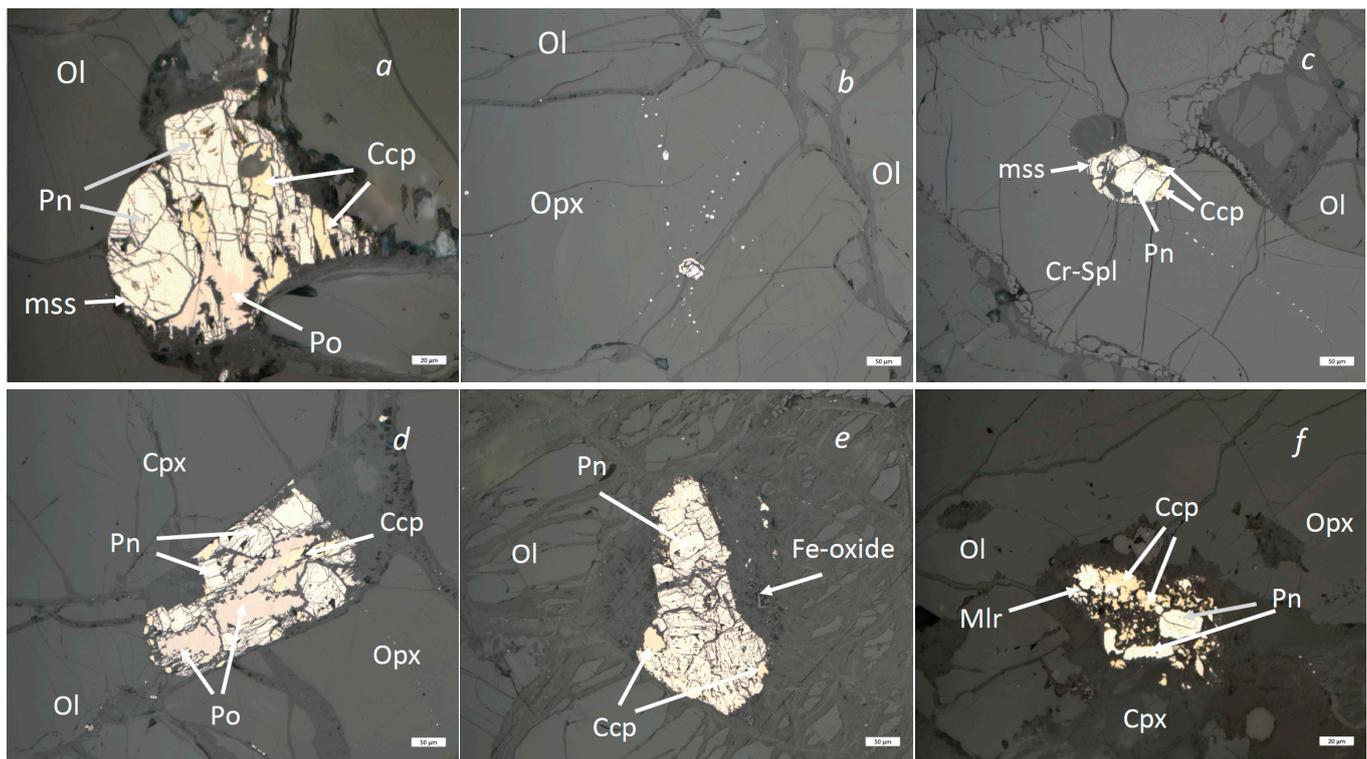
Figure 4. Reflected light photomicrographs of sulfide structural type from Cpx-rich Spl lherzolites: (**a**) three-phase roughly rounded sulfide inclusion (e-type) in Ol. The main body consists of Pn with only insignificant presence of Ccp along the cleavage cracks. Partly preserved pyrrhotite (Po) displays flame-like relations between Pn and Po. Massive Ccp is developed inside the Pn body and at the edges of the inclusion. The scale bar is 20 μm; (**b**) chains of multiple tiny sulfide inclusions (e-type) in Opx developed along the healed cracks in the host mineral. The scale bar is 50 μm; (**c**) oval sulfide inclusion (e-type) in the Spl grain (resorbed edges of the grain are seen). The main volume of the inclusion consists of cleaved Pn with insignificant presence of Ccp along the cleavage cracks. Massive Ccp is developed at the edges of the inclusion. A small mss bleb is present at the edge of the inclusion. Chains of tiny sulfides are located along the existing and healed cracks in Spl. The scale bar is 50 μm; (**d**) irregular three-phase interstitial (i-type) sulfide grain. The main volume consists of Pn + Po often displaying flame-like relations. Ccp forms lamellae along cleavage cracks in Pn. Massive Ccp is developed inside and at the edges of the sulfide grain. The scale bar is 50 μm; (**e**) bi-mineral irregular interstitial (i-type) Pn + Ccp grain with strongly cleaved Pn core and massive Ccp at the edges of the grain. Ccp is sometimes exsolved along the cleavage cracks in Pn. Tiny crystals of Fe-oxides are developed around the sulfide grain. The scale bar is 50 μm; (**f**), resorbed interstitial (i-type) sulfide resulting from the mss breakup. Sulfide consists of equal amounts of massive Pn and resorbed Ccp. Rare patches of Mlr are developed at the edges of sulfide grain. The scale bar is 20 μm.

3.1.3. Sulfides in Spl-Grt Lherzolites

Sulfides here are similar to those from Cpx-rich Spl lherzolites. Major sulfide types are globular inclusions (30–60 μm) in silicate minerals (Figure 5a), big (40–140 μm) irregular grains in kelyphite (Figure 5b), interstitial roughly oval or angular grains that are 30–50 μm in size (Figure 5c,d), and small (10–30 μm) irregular grains in metasomatic veinlets and in silicate-carbonate patches (Figure 5e–g). Sulfide inclusions in silicate minerals are rare, and we analyzed only one such inclusion in sample DN-4. It is a rounded bleb that is 45 × 60 μm in size consisting of a massive cleaved core occupying most of the inclusion and a fragmental rim (Figure 5a). This three-phase inclusion consists of pentlandite (42 wt% Ni, 24 wt% Fe, 0.4 wy% Co, 0.2 wt% Cu) in the core, massive chalcopyrite (33 wt% Cu, 29 wt% Fe, 0.3 wt% Ni) at the edges and in the cleavage cracks in the pentlandite body, and sulfide chemically corresponding to polydymite (51 wt% Ni, 8.0 wt% Fe, 0.4 wt% Co, 39 wt% S) at the outermost part of the inclusion. A three-phase sulfide inside kelyphite (Figure 5b) is represented by a very big grain (70 × 200 μm) that is composed of flame-

like pentlandite (38–41 wt% Ni, 24–28 wt% Fe, 0.3–0.4 wt% Co) occurring inside massive pyrrhotite (58–59 wt% Fe, 1.2–1.9 wt% Ni) and as a cleaved massive species. Chalcopyrite (33–34 wt% Cu, 30–32 wt% Fe, 0.5–0.6 wt% Ni) can be developed as blocky fragments at the edges and inside the dominant pyrrhotite + pentlandite body and/or as fine exsolution lamellae in pentlandite. Grains displaying a very similar structure and composition were observed as i-type sulfides in Cpx-rich Spl lherzolites (Figure 4d). Interstitial sulfides are characterized by their massive and slightly cleaved structure and sometimes a resorbed outer part (Figure 5c,d). Compositionally, the i-type sulfides consist of a pentlandite core (40 wt% Ni, 23 wt% Fe, 0.5 wt% Co, 1.1 wt% Cu), chalcopyrite (33 wt% Cu, 30–31 wt% Fe, 0.3–0.8 wt% Ni) that is either massive or developed along cleavage cracks in the pentlandite body, rear Fe-bearing millerite (61–63 wt% Ni, 2.4–3.3 wt% Fe) along the edges of the sulfide individual, and Ni-rich mss (37–38 wt% Ni, 22–23 wt% Fe) that has been patchily developed along the edges of the sulfide bleb. Occasionally, tiny (<10 μm) Fe oxide crystals are developed next to the interstitial sulfide grains (Figure 5c). As is the case of Cpx-poor Spl lherzolites, Spl-Grt lherzolites display skeletal sulfide crystals that are about 35 × 15 μm in size (Figure 5e) in metasomatic veinlets cross-cutting primary minerals. Skeletal sulfides are represented by two Co-rich phases corresponding to Co-rich violarite, which can be transitional to siegenite (45–53 wt% Ni, 1.1–2.7 wt% Fe, 1.8–8.6 wt% Co) and Co-millerite (1.1–1.4 wt% Fe, 59–62 wt% Ni, 1.0–3.2 wt% Co). Sulfides in metasomatic silicate-carbonate patches are represented by irregular homogeneous and faceted varieties (Figure 5f,g) of pyrite composition (44–46 wt% Fe, 49–50 wt% S, and 41–42 wt% Fe, 43–44 wt% S). A faceted variety of pyrite is characterized by very low totals (85–86%) that suggest a high degree of oxidation.
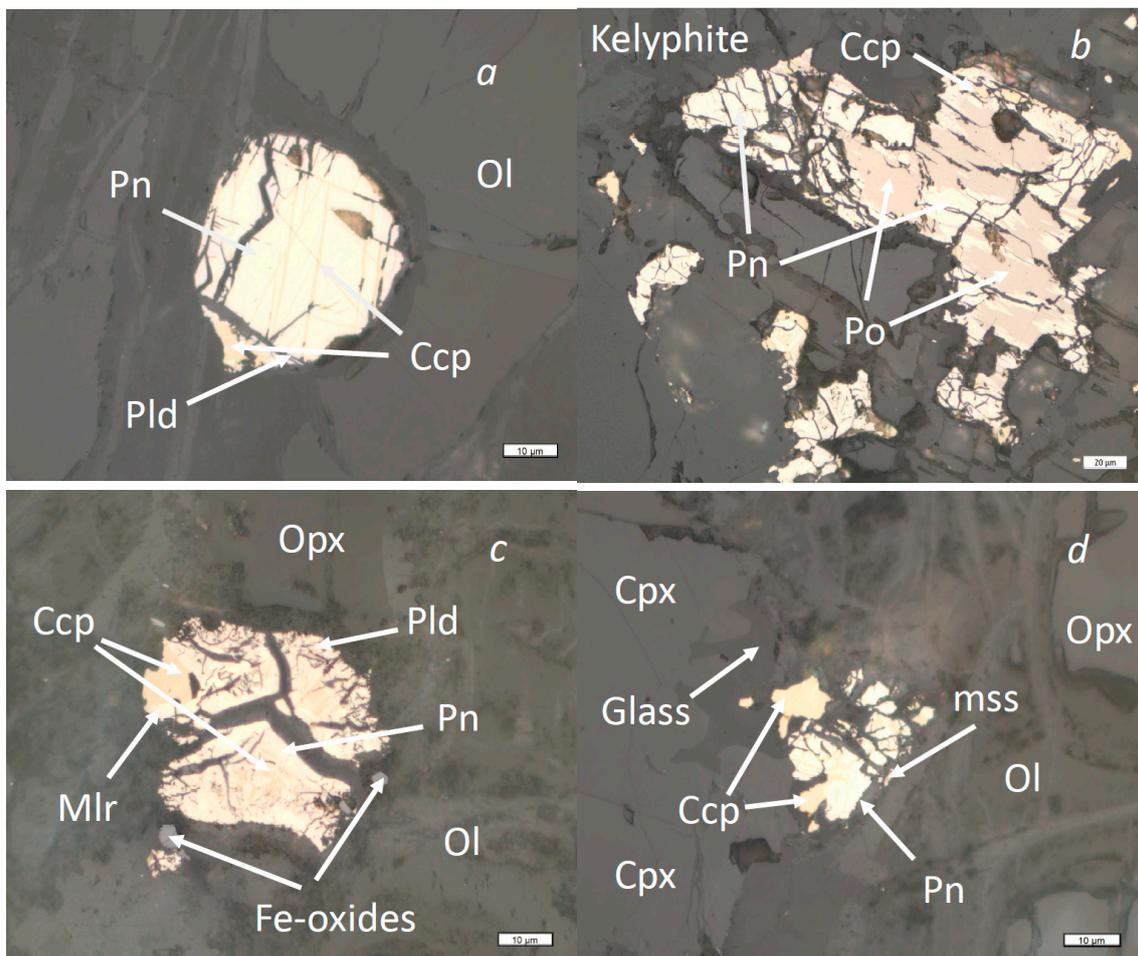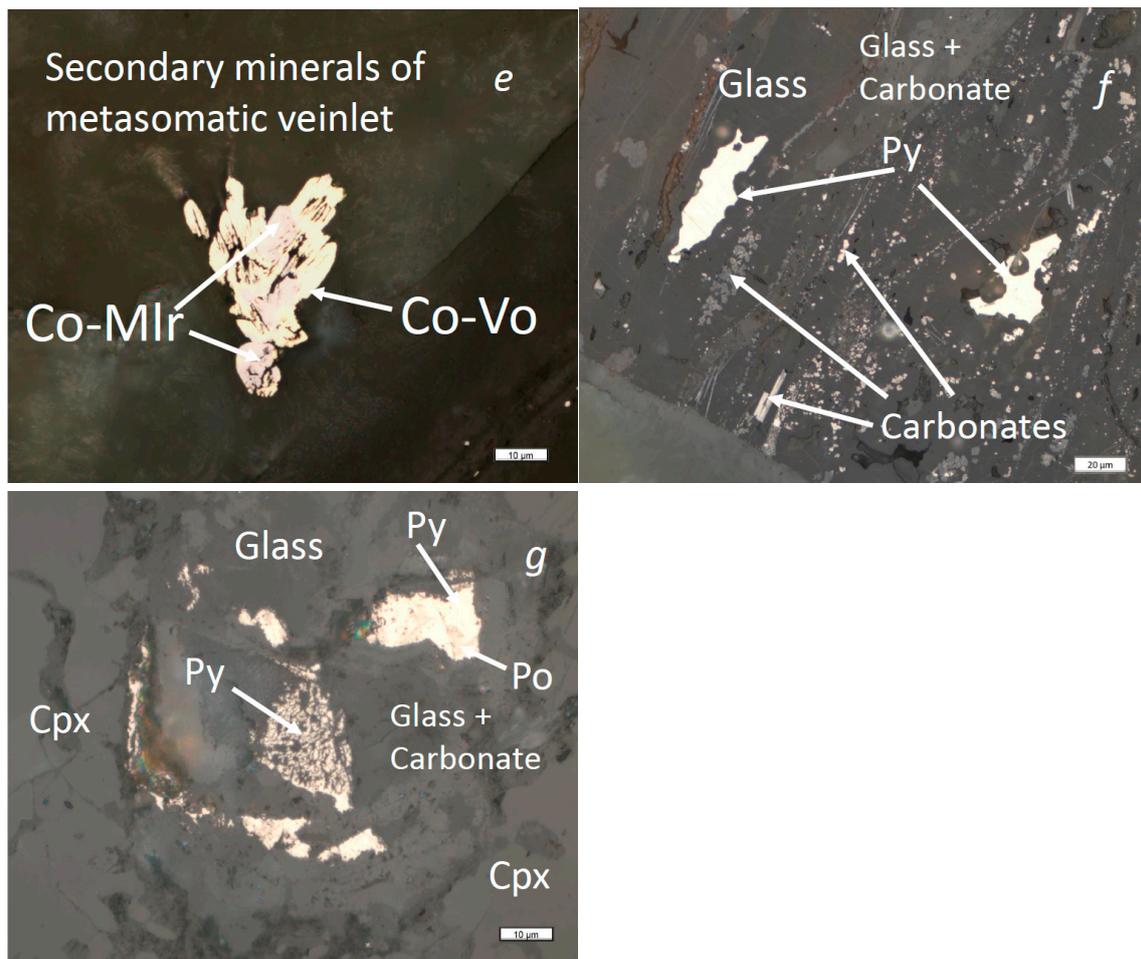

Figure 5. *Cont.*

Figure 5. Reflected light photomicrographs of sulfide structural types from Spl-Grt lherzolites: (**a**) three-phase roughly rounded sulfide inclusion (e-type) in Ol. The main body consists of slightly cleaved Pn with Ccp developed along the cleavage cracks. Rare patches of Pld are present at the edges of the inclusion. The scale bar is 10 μm; (**b**) big irregular sulfide inclusion (e-type) in a kelyphite aggregate. The main volume of the sulfide inclusion is represented by massive Po with flame-like exsolution lamellae of Pn. Massive Pn is developed at the edges of the sulfide inclusion. Insignificant amount of massive Ccp is developed at the edges of the sulfide grain. The scale bar is 20 μm; (**c**) roughly rounded interstitial sulfide (i-type). The main body consists of slightly cleaved Pn with Ccp developed along the cleavage cracks. Rare patches of massive Ccp are present at the resorbed edges of the sulfide grain. Pld patches are present along the edges of the sulfide grain. Small grains of Fe oxides/hydroxide are developed around the sulfide. The scale bar is 10 μm; (**d**) irregular interstitial sulfide (i-type). The main body consists of slightly cleaved Pn with Ccp developed along the cleavage cracks. Massive Ccp is developed at the edges of the sulfide grain. Glass (loci of former silicate melt) is present at the resorbed edge of Cpx. The scale bar is 10 μm; (**e**) skeletal Co-violarite (Vo) + Co-Mlr crystal (m-type sulfide) in a metasomatic veinlet. The scale bar is 10 μm; (**f**) sulfides in a metasomatic carbonate-glassy patch. Irregular blebs of massive pyrite (Py) are clearly seen (m-type sulfide). Tiny crystals of carbonate are present within uncrystallized glassy and carbonate materials. The scale bar is 20 μm; (**g**) assemblage of resorbed and massive sulfides in a metasomatic carbonate-glassy patch (m-type sulfides). Sulfides are represented by bi-mineral (Po + Py) massive grains and faceted monomineral (Py) grains. The scale bar is 10 μm.

3.2. Trace Element Characteristics of Sulfides

Results of the LA-ICP-MS sulfide analyses are summarized in Tables 5 and 6 and in a Supplementary, Table S1. Due to the relatively small size of the sulfide phases that were analyzed, in most cases, the LA-ICP-MS data represent mixtures of the different proportions of two or three sulfide phases, i.e., pyrrhotite (Po), pentlandite (Pn), and chalcopyrite (Ccp). To account for these mixed spectra, results have been grouped according to their major base metal sulfide (BMS) end-member (see Hughes et al. [40]). Analyses with <5 wt.% Ni + Cu are classified as Po; 5–15 wt.% Ni or Cu are Po-Pn or Po-Ccp, respectively; 15–22 wt.% Ni or

Cu are Pn-Po or Ccp-Po, respectively; and analyses with $\geq$22 wt.% Ni or Cu are classified as Pn or Ccp. In results where both Ni and Cu abundances are >5 wt.% each, analyses have been labelled Ccp-Pn or Pn-Ccp (depending on which metal is dominant). This scheme was used further in the Discussion section and in Table S1. In the present section, we consider the trace-element composition of the monomineral sulfides that we were able to analyze.

3.2.1. Sulfides in Cpx-Poor Spl Lherzolites

The only occurrence of BMS big enough to be measured with the LA-ICP-MS is represented here by Ccp-free (<1.0% Cu) pentlandite in a big interstitial sulfide bleb (sample U-3/4-2) and low-Fe pentlandite and polydymite in a roughly oval interstitial sulfide bleb (sample U-1/4-3). Pentlandite is characterized by a high concentration of Se (511 ppm), Mo (1541 ppm), and Te (86 ppm). Concentrations of elements such as Cd, In, and Sn are very low (down to below the detection limit for Cd). The total concentration of the PGE is moderately high (204 ppm) with a very high concentration of Pd (156 ppm). The mineral is poor in the I-PGE (Ru, Rh, Os, Ir) with 0 < Os < 5 ppm and is strongly enriched in the P-PGE (Pd and Pt) relative to the I-PGE (($Pd/Ir)_N$ = 112) (normalized to the CI chondrite; [41]). The second occurrence, low-Fe (<8% Fe) and high-Ni (>55% Ni), a variety of pentlandite occurs in a rounded interstitial sulfide bleb (Figure 3c). The low-Fe pentlandite is characterized by high concentrations of Ge (64 ppm), Se (198 ppm), Te (25 ppm), and Pb (318 ppm). Elements such as Cd, In, and Sn display very low concentrations (down to below the detection limit for In) that are similar to those observed in regular pentlandite. Concentrations of the PGE are moderate (total 68 ppm) with a very low concentration of Rh (0.60 ppm). The mineral is overall poor in the I-PGE (0 < Os < 5 ppm) and is significantly enriched in the P-PGE relative to the I-PGE (($Pd/Ir)_N$ = 19).

Polydymite from the resorbed edge of the same sulfide bleb (Figure 3c) is characterized by elevated concentrations of Pb (290 ppm) and Ag (48 ppm) and by quite high concentrations of the PGE (total 62 ppm) with a significant contribution of Pt (23 ppm). The mineral is characterized by the low I-PGE concentrations (0 < Os < 5 ppm) and is enriched in the P-PGE relative to the I-PGE (($Pd/Ir)_N$ = 19). Among the minor sulfide types, interstitial Ni-Cu mss (sample U-1/4-3) displays high concentrations of most trace elements. It is especially pronounced for Mo (43–44 ppm), Te (47–74 ppm), and the PGE. The high total PGE concentrations of 519–596 ppm are mostly due to very high concentrations of Pd (304–422 ppm) and Ir (69–86 ppm). In spite of the high Ir concentrations, Cu-Ni mss is poor in Os (1 $\leq$ Os $\leq$ 5 ppm) and only insignificantly enriched in the P-PGE relative to the I-PGE (($Pd/Ir)_N$ = 2–3). Co-violarite from the Co-millerite to Co-violarite aggregates (structurally similar mineral was described by Huges et al. [40] in lherzolite xenoliths from Scotland as Co-millerite) in metasomatic veinlets displays high concentrations of Co (2.5–2.6%, as measured by the LA) and sometimes elevated concentrations of Cr (up to 890 ppm), Ag (up to 33 ppm), As (52–92 ppm), Pt (5.6–11.6 ppm), and Pb (49–57 ppm). Co-violarite has moderately low I-PGE concentrations (1 < Os < 10 ppm), and it does not show P-PGE enrichment relative to the I-PGE (($Pd/Ir)_N$ = 0.7–1.7).

3.2.2. Sulfides in Cpx-Rich Spl Lherzolites

Pyrrhotite is overall characterized by the lowest concentrations of trace elements among all of the BMS that were studied (Table 5). Only the Mn (319 ppm), Se (98 ppm), Mo (33 ppm), and Zn (12 ppm) in pyrrhotite displayed concentrations similar to or even higher than those measured in other BMS (the only monomineral pyrrhotite analyzed from the i-type sulfide). The rest of the trace elements (except for Co; 77 ppm) displayed concentrations in the range of 0.5–2 ppm.

Concentrations of the PGE are low (total is 2.5 ppm). The concentrations of the I-PGE were likewise low (0 < Os < 5 ppm), and the enrichment of the P-PGE relative to the I-PGE was not high (($Pd/Ir)_N$ = 0.2).

Pentlandite is characterized by insignificantly higher concentrations of trace elements compared to those in pyrrhotite. The only difference is the expectedly much higher

concentrations of Co in pentlandite (4500–5990 ppm in e-type sulfides and 5080–8880 ppm in i-type sulfides). Pentlandite from the inclusion in spinel is characterized by very low (evidently, the lowest among all studied BMS) concentrations (often below the detection limit) of Zn, Ga, Ge, Cd, In, Sn, and Sb. Pentlandite displays moderate total concentrations of the PGE (9–52 ppm with the highest concentrations of inclusion in Spl). The mineral is characterized by very low concentrations of the I-PGE ($0 \leq Os << 5$ ppm) and by a varying degree of the enrichment of the P-PGE relative to the I-PGE ($(Pd/Ir)_N = 0.4$–8.0 in e-type sulfides and 11.6–64.8 in i-type sulfides), with the lowest degree displayed by pentlandite from the inclusion in spinel.

Chalcopyrite is characterized as elevated relative to other BMS total and individual concentrations of trace elements (Table 5), with Zn concentrations being significantly higher in chalcopyrite (827–2030 ppm). The PGE display uniformly elevated concentrations of the total PGE concentrations varying from 9 to 40 ppm. The mineral is characterized by the moderate enrichment of the I-PGE ($1 < Os < 5$ ppm) and by the virtual absence of the P-PGE enrichment relative to the I-PGE ($(Pd/Ir)_N = 0.2$–2.0). Unlike the other BMS, chalcopyrite from the pentlandite + chalcopyrite inclusion in the Cr-spinel displays high concentrations of Ti (424 ppm) and Cr (5659 ppm).

Table 5. Trace-element characteristics of monomineral BMS in lherzolites from East Antarctica (ppm).

Rock	Cpx-Poor						Cpx-Rich		
	Inter						In Spl		In Ol
Sample	U-3/4-2			U-1/4-3			UN-1		XLT-4
Mineral	Pn	Low-Fe Pn	Pld	Cu-Ni ss	Cu-Ni ss	Pn	Pn	Ccp	Pn
Ti	7.08	nd	nd	nd	nd	nd	nd	423.7	230.2
Cr	9.04	nd	nd	nd	nd	nd	nd	5659	401.8
Mn	4.71	3.43	3.12	1331	359.4	31.81	48.64	2122	337.7
Co	2782	20.65	1880	3159	2562	4506	5442.5	109.2	5989
Ni	361,633	551,976	502,298	466,104	351,212	318,362	331,828	19,670	353,381
Cu	8231	23.68	21.44	152,811	194,705	387.2	335.6	212,253	11,938
Zn	7.74	4.77	4.34	bdl	bdl	4.43	bdl	2030	37.62
Ga	0.45	0.68	0.25	0.39	bdl	bdl	bdl	13.84	2.30
Ge	5.05	64.40	58.60	17.18	7.27	1.66	bdl	48.56	22.32
As	99.14	39.38	35.84	36.65	20.79	2.64	3.36	38.35	12.07
Se	511.2	197.6	179.8	352.6	413.4	112.5	108.3	204.8	167.0
Mo	1541	1.45	1.32	44.32	43.17	14.65	16.39	15.09	18.32
Ru	27.16	1.92	1.75	24.93	77.51	8.73	10.30	21.91	1.10
Rh	8.60	0.60	0.55	58.43	41.66	1.31	1.63	2.42	0.43
Ag	20.54	52.45	47.73	73.82	58.72	7.99	14.20	15.72	19.12
Pd	156.0	37.51	34.13	422.1	303.8	1.76	32.50	7.36	2.81
Cd	bdl	2.16	1.96	1.63	bdl	bdl	bdl	15.61	8.41
In	0.06	bdl	bdl	bdl	bdl	bdl	bdl	0.92	0.47
Sn	1.08	0.39	0.36	0.84	bdl	0.69	0.39	15.67	4.02
Sb	4.44	2.01	1.83	1.24	2.08	bdl	bdl	4.85	1.65
Te	86.01	24.78	22.55	46.99	74.07	6.71	7.03	47.48	bdl
Re	0.40	1.72	1.57	0.17	0.10	5.83	6.11	1.90	0.68
Os	0.95	0.83	0.75	1.47	5.33	0.58	0.66	1.13	bdl
Ir	0.67	0.98	0.89	68.79	86.06	4.20	4.37	3.11	0.30
Pt	10.32	25.76	23.44	20.59	5.09	2.13	2.60	4.39	1.33
Au	0.16	0.60	0.55	14.30	12.73	0.53	7.40	1.59	0.13
Pb	46.51	318.4	289.7	142.3	96.99	0.49	0.69	9.82	24.45
Bi	7.58	0.43	0.39	0.82	0.60	0.52	0.22	4.62	1.62

Table 5. *Cont.*

Rock	Cpx-rich						Spl-Grt
	Inter						
Sample	UN-1					XLT-4	DN-1
Mineral	Pn	Pn	Pn	Po	Ccp	Ccp	Pn
Ti	44.43	39.07	18.16	nd	78.03	3.87	17.61
Cr	43.14	76.56	157.1	nd	71.26	42.66	109.8
Mn	104.5	50.49	40.87	318.6	31.46	4.17	609.9
Co	8879	5077	5649	76.90	4.58	106.9	3080
Ni	281,295	329,743	341,584	11,073	bdl	52.59	349,622
Cu	1106	136.1	104.9	763.0	370,433	324,917	8631
Zn	44.32	14.31	10.36	12.31	827.1	1048	333.8
Ga	1.52	1.91	0.91	0.47	2.55	0.35	0.98
Ge	14.29	12.95	8.04	bdl	33.54	3.08	18.17
As	12.98	8.31	6.13	bdl	26.54	2.20	6.20
Se	72.27	82.92	235.2	97.91	266.4	129.9	267.6
Mo	12.71	30.07	15.44	33.31	7.85	1.08	2.28
Ru	1.11	1.04	bdl	bdl	bdl	6.08	21.11
Rh	0.16	bdl	0.08	0.19	1.65	1.96	0.18
Ag	9.63	1.55	6.92	0.51	1.88	0.47	26.98
Pd	11.15	2.85	7.51	0.13	2.17	0.48	48.02
Cd	bdl	bdl	2.64	0.39	84.05	11.35	bdl
In	0.46	0.15	bdl	bdl	0.36	0.45	0.16
Sn	6.96	2.53	2.09	bdl	4.48	2.85	2.15
Sb	1.71	1.62	0.70	bdl	3.22	0.47	7.56
Te	bdl	bdl	4.07	1.29	175.7	1.94	8.66
Re	2.85	0.38	6.79	1.20	0.50	0.44	0.10
Os	1.77	0.42	bdl	1.19	1.34	4.30	13.30
Ir	0.25	0.21	0.10	0.57	bdl	2.62	1.86
Pt	7.72	4.34	1.30	0.43	3.62	0.52	2.45
Au	0.24	bdl	0.09	bdl	0.70	0.08	bdl
Pb	20.48	9.04	27.24	0.70	4.87	4.38	36.19
Bi	2.03	1.22	2.85	0.64	2.89	0.56	1.65

nd, no data available; bdl, below the detection limit.

3.2.3. Sulfides in Spl-Grt Lherzolites

The only monomineral BMS that was analyzed in the Spl-Grt lherzolites for trace element concentrations was pentlandite from the i-type sulfide (Figure 5a). Additionally, sheer Co-violarite in metasomatic veinlets and pyrite in silicate-carbonate patches were analyzed (Figure 5e,f). Interstitial pentlandite, which can be considered as Ccp-free (<1.0% Cu), is characterized by high concentrations of Se (268 ppm) and Ag (27 ppm) and by low concentrations of Mo (2.3 ppm). Concentrations of other trace elements are generally similar to those in pentlandite from other lherzolite types (Table 5). Very high concentrations of the I-PGE (Os > 10 ppm) and enrichment in the P-PGE relative to the I-PGE ((Pd/Ir)$_N$ = 13) are typical for pentlandite.

Co-violarite from skeletal crystals displays high concentrations of Co (2.5–3.3% as measured by the LA) and sometimes elevated concentrations of Cr (371–735 ppm), As (690–740 ppm), and Sb (9–14 ppm). The mineral has moderately low concentrations of the PGE (total 8–12 ppm), and while it is characterized by a very low I-PGE content (Os is below the detection limit), it is only insignificantly enriched in the P-PGE ((Pd/Ir)$_N$ = 3–5) because concentrations of Pd are low and are generally comparable to those of Ir (Table 6). The pyrite from silicate-carbonate patches is characterized by varying amounts of Zn (4–396 ppm) and Ge (12–149 ppm) and by very low total concentrations of the PGE (0.8–1.5 ppm), which is consistent with the very low I-PGE content (0 < Os < 0.5 ppm) and the total absence of Ir.

Table 6. Trace-element characteristics of m-type sulfides in lherzolites from East Antarctica (ppm).

Rock	Cpx-poor			Spl-Grt				
	Skeletal			Faceted	Massive		Skeletal	
Sample	32601-9b			DN-4				
Mineral	Co-Vo	Co-Vo	Co-Vo	Py	Py	Py	Co-Vo	Co-Vo
Ti	46.40	29.47	11.03	15.34	16.56	10.66	117.3	71.59
Cr	889.8	62.98	149.8	397.3	97.08	7.23	735.4	371.1
Mn	168.1	30.13	23.41	4634	1529	3.70	24.59	36.91
Co	24,794	25,662	24,616	113.2	76.95	0.60	24,106	32,944
Ni	487,469	480,393	521,611	137.8	1002	55.87	553,276	540,826
Cu	9332	18,647	13,891	24.84	101.1	8.03	106.2	2355
Zn	97.58	189.5	35.85	395.6	49.89	3.54	24.71	42.19
Ga	2.01	2.54	0.84	0.68	0.52	0.53	2.65	3.59
Ge	13.70	19.49	11.15	148.9	32.35	11.52	35.13	40.04
As	51.71	72.89	92.34	10.57	8.40	3.46	739.2	689.6
Se	134.0	273.1	122.0	bdl	38.79	20.04	60.21	109.0
Mo	23.38	23.59	41.87	0.85	1.73	0.49	5.36	4.85
Ru	8.40	7.81	3.22	bdl	bdl	bdl	bdl	bdl
Rh	1.46	1.47	0.66	0.16	0.19	0.12	0.50	0.88
Ag	33.36	30.70	27.95	0.47	1.36	0.19	1.84	1.85
Pd	6.19	17.93	7.73	0.92	1.15	0.60	2.90	6.80
Cd	bdl	9.88	11.12	3.46	bdl	bdl	bdl	19.75
In	0.15	0.22	0.15	0.09	bdl	0.07	1.46	bdl
Sn	2.62	2.19	1.25	6.79	2.85	0.74	5.36	8.90
Sb	1.55	0.82	2.81	0.30	0.45	0.24	9.48	13.72
Te	7.94	33.94	12.74	4.46	bdl	2.56	bdl	bdl
Re	0.50	0.68	0.90	0.11	0.17	0.07	bdl	bdl
Os	5.78	6.18	2.07	0.31	bdl	bdl	bdl	bdl
Ir	4.13	5.15	2.58	bdl	bdl	bdl	0.48	0.61
Pt	6.53	11.60	5.65	0.85	1.28	0.48	3.08	2.79
Au	0.90	2.71	0.86	0.19	bdl	0.16	0.85	1.11
Pb	56.59	51.24	48.62	0.25	0.51	0.07	2.03	2.68
Bi	1.06	1.38	0.63	0.55	0.71	0.31	1.81	3.03

4. Discussion

A broad spectrum of sulfide mineral assemblages in the SCLM lherzolite xenoliths from the Jetty Peninsula can be explained by the presence of sulfides from different environments such as the xenolith matrix, metasomatic veinlets, and carbonate-silicate patches. Previously described occurrences of BMS in lherzolite xenoliths from other localities (e.g., Dromgoole and Pasteris ([19–21,25] and references therein)) are also common in the studied Antarctic xenoliths. Other types of sulfides in the lherzolites from the Jetty Peninsula are less common and are poorly studied. The only study so far targeting sulfides from East Antarctic SCLM xenoliths showed that the e-type sulfides contain assemblage of quenched sulfide melt and mss in which Ni is more abundant than Fe [11].

4.1. Sulfides from Lherzolite Matrix

Most investigators assume that sulfide inclusions in the minerals of lherzolite matrix represent immiscible sulfide liquid that was trapped during the crystallization of peridotite minerals, whereas interstitial sulfides formed after the crystallization of the primary lherzolite minerals, i.e., during sulfide liquid migration along the cracks and mineral seams (see Solovova et al. [11], Kiseeva and Wood [15], Griffin et al. [18], Sen et al. [24], Mitchell and Keays [42]). However, Dromgoole and Pasteris [19] suggested that the often-observed lack of compositional differences between the e- and i-type sulfides could indicate that the creation of these sulfides was mainly due to the incorporation of postmetasomatic sulfur-bearing and CO_2-rich melts. The present study allows new insight into these processes.

Compositions of the studied BMS from the lherzolite matrix lie within both the mss and the mss + Liq fields of the Fe-(Ni + Co)-S system (Figure 6). After mss (Fe-rich and Ni-poor) begins to crystallize at 1190 °C from Ni-Cu-Fe sulfide liquid, residual sulfide liquid gradually enriches in Ni relative to Fe [43–46]. Therefore, in the S-rich of the studied lherzolites system at the suggested ambient temperatures suggested for most varieties of those lherzolites (1030–1180 °C), mss of an overall pyrrhotite composition is the only possible solid phase coexisitng with the Ni-Cu-Fe sulfide liquid [21]. The maximum content of Cu (7%) would be reached at 1000 °C [21]. With further cooling, chalcopyrite starts to crystallize at 960 °C, and when the temperature decreases to 900 °C, the stability field of the solid phase (i.e., mss) precipitating from the sulfide liquid spans the entire FeS-(Ni + Co)S connection with slightly less Cu dissolving in it [21]. Therefore, the mss and possibly high-temperature pentlandite could coexist with the sulfide liquid in lower-temperature (down to 850 °C) varieties of Cpx-poor lherzolites (see Kitakaze and Komatsu [47]). Furthermore, the Cu-bearing mss underwent a subsolidus breakup of the Cu-poor mss + Cu-rich phase (Ccp) at temperature of 500–600 °C [25]. Pentlandite, a major constituent of sulfide assemblages in the lherzolite matrix, starts to crystallize from the mss at 610 °C, and it is stable in the Fe–Ni–S system below this temperature [21,48]. The remnants of the Ni-rich mss along the edges of the Ccp + Pn blebs decomposes when the temperature is below 380 °C. It forms stoichiometric NiS, which breaks-up to form millerite (NiS) and/or polydymite (NiNi$_2$S$_4$) at temperatures of ~300 °C [21]. With this, the transformation of e-type sulfides ends. For the i-type sulfides with stable chalcopyrite stable, the Cu-poor/free and Ni-bearing mss underwent further low-temperature transformation. A high-temperature assemblage experiences a separation of Ccp + mss break up to create Po + Pn when the temperature is below 300 °C. Flame-like pentlandite in pyrrhotite matrix (Figures 4d and 5b) becomes a product of the mss break up, likely due to homogeneous Ni nucleation at temperatures between 150 and 300 °C [20,49,50].

In summary, the BMS assemblages in the Jetty Peninsula lherzolite xenolith matrix are products of the subsolidus re-equilibration of high-temperature mss crystallized from the sulfide liquids that are mainly of FeS composition but that also contain Cu, Ni, and Co (see Bishop et al. [51]). In the studied rocks, all BMS display typical recrystallization features such as aggregates, lamellar exsolutions, flame-like structures, and low-temperature phase assemblages (Po + Pn + Ccp), suggesting that the studied sulfide assemblages are not of primary mantle origin. The rare presence of a patchy mss around the pentlandite-chalcopyrite cores suggests that these assemblages have not reached full equilibrium and that subsolidus equilibration stopped at temperatures around 300 °C. Observed flame-like pentlandite in the pyrrhotite matrix suggests that the mss breakup completely finished at temperatures between 150 and 300 °C.

4.2. Sulfides from Silicate-Carbonate Patches

One line of evidence of melt incorporation into the lherzolite matrix is the existence of silicate-carbonate patches (Figure 5f,g). These patches contain pyrite and represent the loci of former immiscible silicate-carbonate-sulfide liquid. The former existence of carbonate melts was clearly distinguished by the presence of calcite, dolomite, apatite, and magnesite in some lherzolite xenoliths from the Jetty Peninsula [4]. Pyrite from silicate-carbonate patches could represent loci of former Fe-S liquid that existed immiscibly with the silicate and carbonate liquids. The quench structure of these patches suggests the very fast cooling of the liquids, while the presence of pyrite indicates the lower temperature limit for the fluid before quenching since pyrite is unstable above ~740 °C [19,21]. A detailed study of these patches was, however, beyond the scope of the present investigation, and here we deal only with their sulfide component (see sections below).
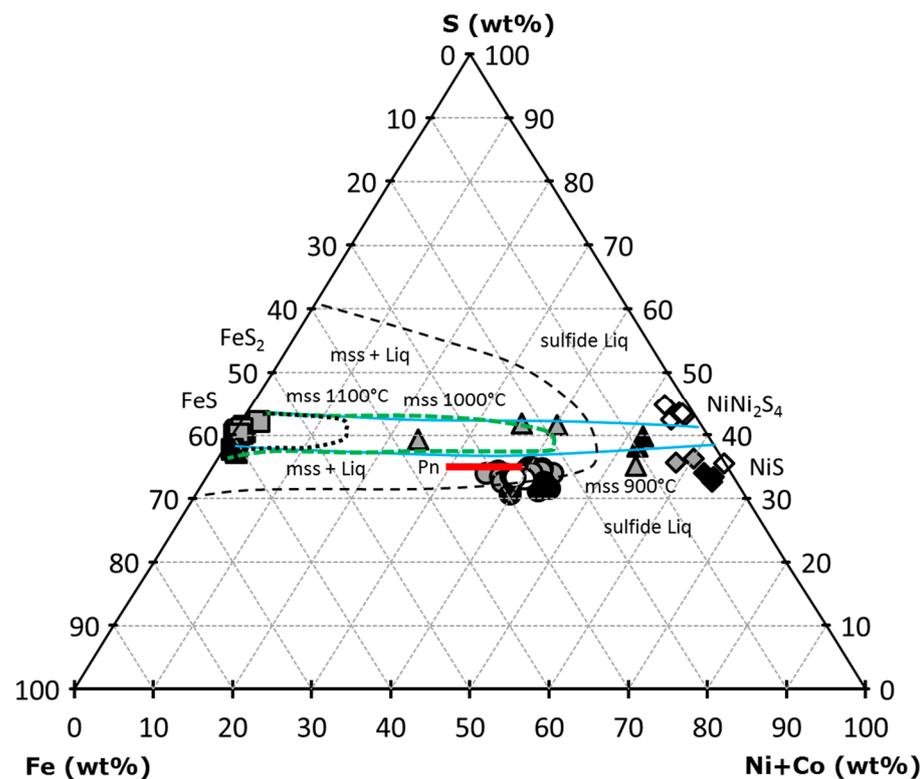
Figure 6. Composition of sulfides in the Fe-(Ni + Co)-S (wt%) system. The high-temperature (1100–900 °C) phase relations are after Killerud et al. [48]. The green dashed line borders a field where mss coexists with sulfide liquid at 1000 °C. The thin dashed line borders sulfide liquid field from that of mss + liq at 1000 °C (after Shindo et al. [13]). Empty symbols are for sulfides from Cpx-poor Spl lherzolites; grey symbols are for sulfides from Cpx-rich Spl lherzolites; solid symbols are for sulfides from Spl-Grt lherzolittes. Circles are for Pn, squares are for Po, triangles are for the mss, diamonds are for Pld and Mlr. Sulfides of the e- and i-types do not show significant compositional differences in this system. Pentlandite composition range is based on Alard et al. [17].

4.3. Sulfides from Metasomatic Veinlets

Another interesting feature is the presence of metasomatic veinlets cross-cutting the primary minerals in some xenoliths. Such veinlets contain minerals such as apatite, calcite, Fe-rich dolomite, ferroan magnesite, Ba-Ti-rich and Ba–Ti-poor mica, and humite-group minerals (see Kogarko et al. [9]). We found that such veinlets also contain a sulfide phase that is significantly different from the BMS in the lherzolite xenolith matrix, i.e., skeletal crystals of Co-millerite + Co-violarite (see Hughest et al. [40], and Nkoumbou et al. [46]). The formation temperature for such assemblages was just above 350 °C [52], which was close to the blocking temperatures of the subsolidus reactions in the BMS from the lherzolite marix. Such temperatures suggest that low-temperature metasomatism occurred at crustal levels. A detailed study of the veinlets was beyond the scope of the present investigation.

4.4. Trace Elements in Lherzolite Sulfides

Since multiphase sulfide assemblages as they appear in the samples studied are not of primary mantle origin, some compositional features intrinsic to the parental sulfide liquids could have been lost during the low-temperature breakup of the mss. However, trace elements often behave conservatively, keeping the compositional features of the primary material. Although the majority of information on mantle sulfides from elsewhere is derived from the PGE, we also considered the concentrations and distributions of trace elements that suggest histories of both depletion and re-enrichment in the host mantle rocks, which is consistent with observations made by Foley et al. [4], for example.

4.4.1. Platinum Group Elements

The PGE are highly conservative elements that may carry information on processes such as melting, sulfide precipitation, and sulfide addition via metasomatism in the upper mantle (see Alard et al. [17]). Bulk lherzolite xenoliths from East Antarctica display non-fractionated PGE patterns with concentrations of the PGE that are mostly around 0.01 × CI chondrite [53]. Such low PGE concentrations are consistent with studies by Kiseeva and Wood [15], Griffin et al. [18], Mitchell and Keays [42], and many others who show that sulfides are the main host phases for the PGE in the upper mantle rocks.

The PGE from the studied sulfides can be grouped according to the distribution pattern styles (Figure 7a–g): (a) subdued convex down I-PGE patterns followed by a deep trough at Pt; (b) convex up PGE patterns for the I-PGE followed by a deep trough at Pt and a peak at Pd; (c) almost unfractionated PGE patterns and ≥10 × CI chondrite PGE concentrations; (d) significantly fractionated PGE patterns often characterized by troughs at Ir and Pt and with PGE concentrations varying from chondritic to ≥10 × CI chondrite; (e) significantly fractionated PGE patterns often characterized by a trough at Ir; (f) "M"-shaped PGE patterns and strong enrichment in Pd with overall high PGE concentrations (up to ~1000 × CI chondrite)—this pattern is typical for the Cu-Ni mss; and (g) almost unfractionated and sometimes incomplete PGE patterns typical of m-type sulfides.
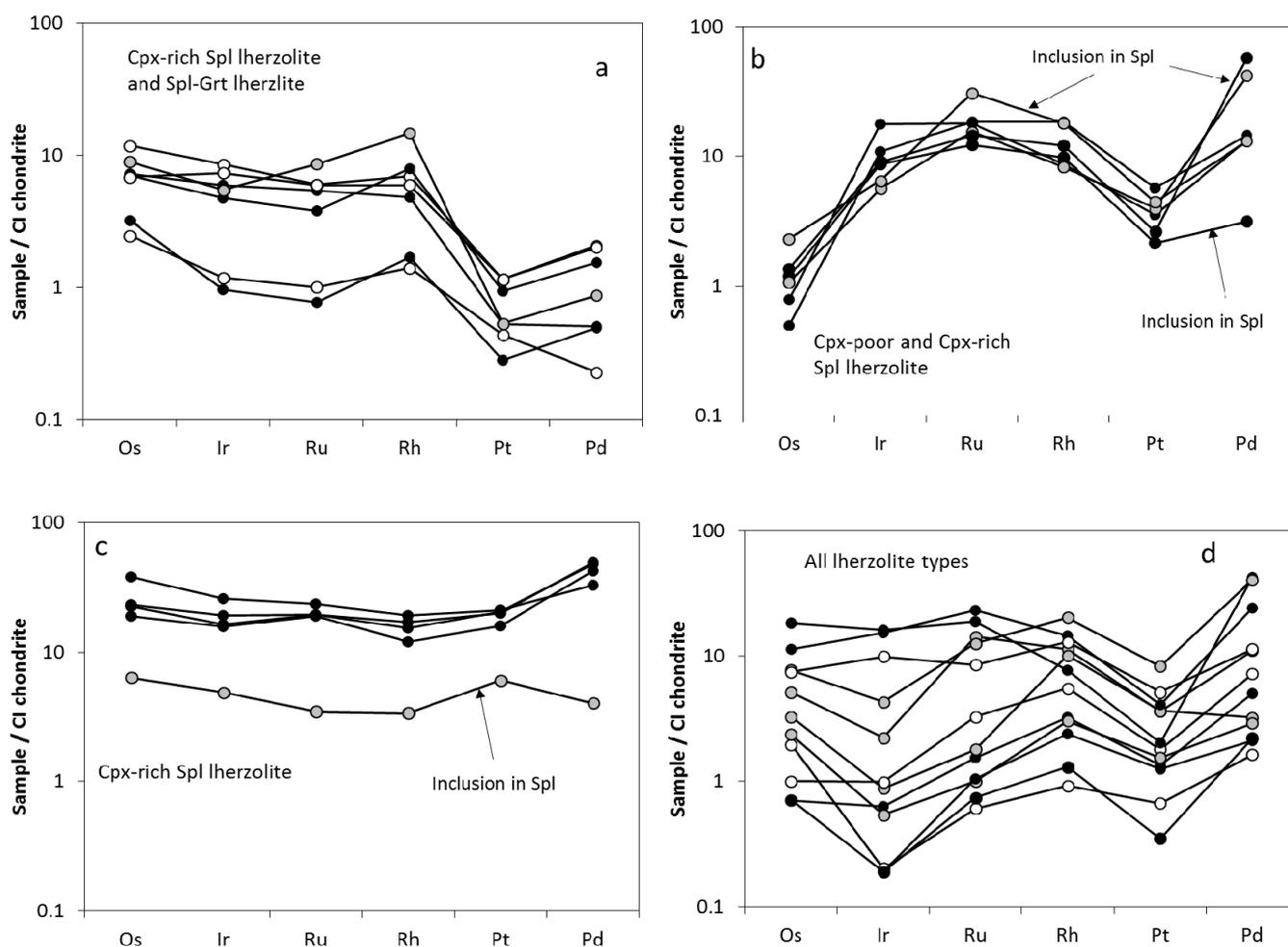
Figure 7. *Cont.*
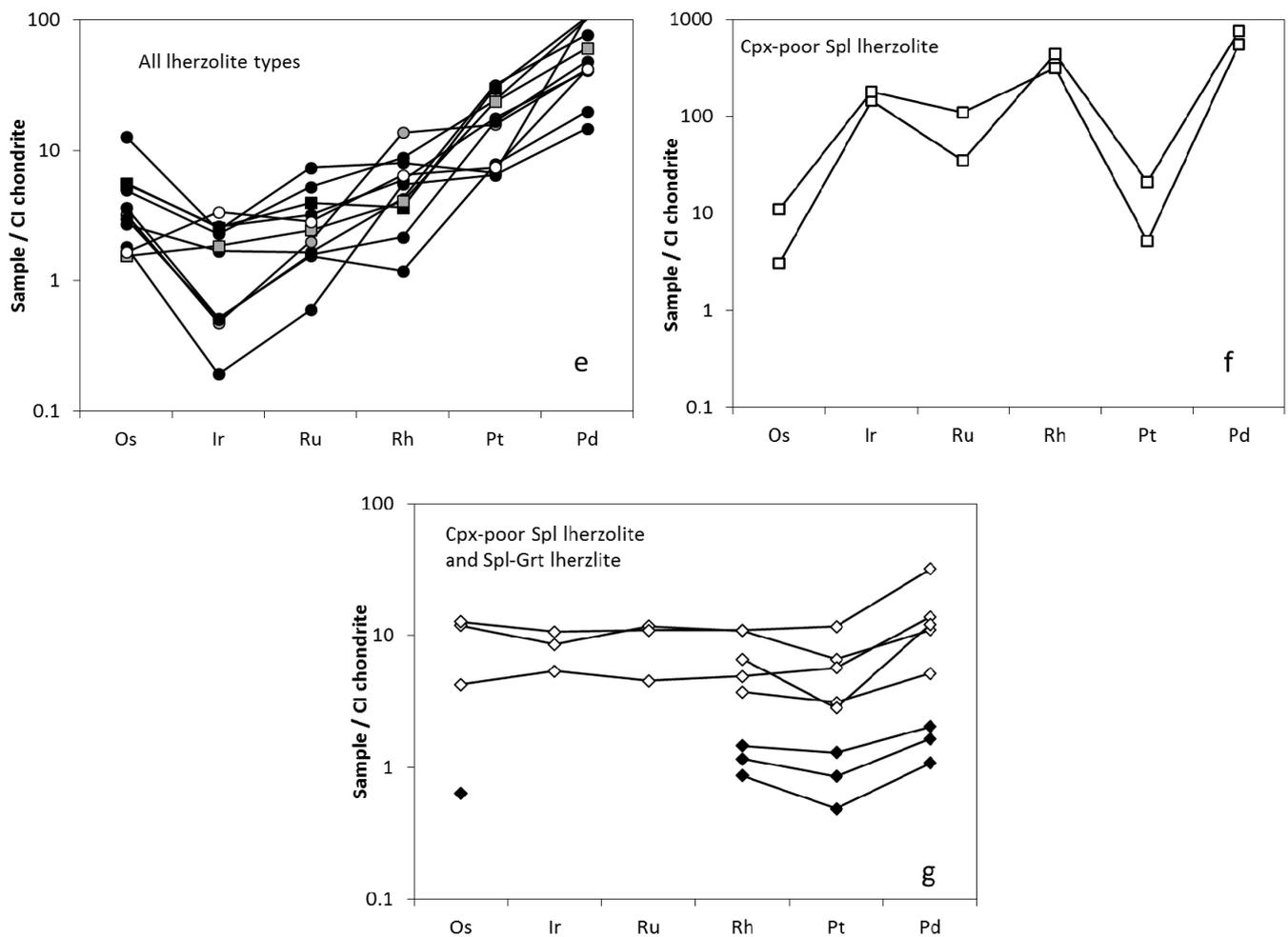
Figure 7. CI chondrite-normalized PGE patterns for the studied sulfides (CI chondrite composition is after Anders and Grevesse [41]). (**a**) Unmetasomatized residual sulfides of the e- and i-types from Cpx-rich Spl lherzolites and Spl-Grt lherzolites. Stepped distribution of the PGE is displayed by Pn (black circles), Ccp (grey circles), and Po (open circles) from a huge interstitial sulfide grain from Cpx-rich Spl lherzolite (see Figure 4d) and a huge sulfide grain included in Kel in Spl-Grt lherzolite (see Figure 5b). Almost unfractionated PGE distribution is observed for Ccp from an outer part of the inclusion in Spl (see Figure 4c), which is probably due to infiltration of immiscible sulfide melt from outside the Spl grain (cf. Figure 6c); (**b**) convex up PGE distributions in Pn and Ccp from sulfides of the e-type (in Spl and Ol) in Cpx-poor Spl lherzolite and in Cpx-rich Spl lherzolite (see Figures 3b and 4c); (**c**) almost unfractionated PGE patterns of Pn from sulfides of the i-type in Cpx-rich Spl lherzolite (see Figure 4e,f). These compositions could correspond closely to the initial stages of the mss break up; (**d**) insignificantly fractionated PGE patterns for Pn, Ccp, and Po from the e- and i-type sulfides in all three studied lherzolite types. The patterns are characterized by chondritic to suprachondritic PGE concentrations complicated by depletion in Pt and enrichment in Pd (see text for details); (**e**) strongly fractionated PGE patterns for Pn (low-Fe pentlandite is balck squares), Ccp, Po, and Pld (grey squares) from the i-type sulfides in all three studied lherzolite types. For most of these sample, an asymmetric "U"-shaped pattern due to fractionation of Ir relative to Os is typical; (**f**) convex up PGE patterns (complicated with a trough at Ru) from the Cu-Ni mss in Cpx-poor Spl lherzolite). Strong enrichment in Pd is observed (see text for details); (**g**) almost unfractionated PGE patterns (partly incomplete) for the m-type sulfides. PGE concentrations vary from chondritic (Py from silicate-carbonate patches; black diamonds) to around 10 × CI chondrite (Co-Vo from metasomatic veinlets; open diamonds).

Overall, distinguishing different sulfide populations can be done on the basis of relations between the I-PGE and the P-PGE. The residual PGE signatures are evident from (Pd/Ir)$_N$ ratio < 1, whereas (Pd/Ir)$_N$ > 1 suggests metasomatic influence [27]. Typically, the (Pd/Ir)$_N$ ratios in the e-type sulfides are much lower, and Os and Ir abundances are higher than those for the i- and m-type sulfides. This records melting processes in the

e-type sulfides, while the i- and m-type sulfides have PGE patterns suggesting precipitation from silicate melts or the introduction of other forms of metasomatism [11,15,24,27]. Additionally, the relationship between Pt and Pd in residual sulfides provides information re- equilibration with the initially depleted melt portion in Pd sulfides, (inducing $[Pt/Pd]_N$ to be <1 [27]). The time-resolved laser ablation signals on sulfides mostly did not show any irregularities for the PGE. This is strong evidence that most PGE are rather evenly distributed throughout the sulfide phase than grouped in individual clusters.

Only a few of the studied e-type sulfide grains in Cpx-poor Spl lherzolite displayed residual PGE signatures $((Pd/Ir)_N = 0.74–1.33$, and 7.45 for Ccp) with insignificant secondary re-enrichment $([Pt/Pd]_N = 0.27–0.39$ and 0.09 for Ccp). These sulfides are characterized by convex up PGE patterns with Ir_N over Os_N (Figure 7b). On the contrary, the domination of the P-PGE over the I-PGE $((Pd/Ir)_N = 3–28)$ suggests that almost all i-type sulfides in Cpx-poor Spl lherzolites can be considered as precipitated from melts that have migrated through the lherzolite matrix. The PGE patterns for these sulfides vary from insignificantly fractionated and similar to those observed for the e-type sulfides, but with Os_N over Ir_N (Figure 7d), to fractionated with the P-PGE strongly enriched over the I-PGE (Figure 7e). Interesting features are displayed by the interstitial Cu-Ni mss. They are characterized by extremely high concentrations of the PGE (519–596 ppm) where Pd strongly prevails (304–422 ppm). Anomalously high concentrations of Ir (69–86 ppm) accompanied by low concentrations of Os (1.5–5.3 ppm) suggests a state of disequilibrium and rapid solidification of the Cu-Ni mss. High Ir concentrations that are inconsistent with low Os concentrations may also suggest that sulfide liquid of such composition could be parental to the Ir-bearing sulfides of the Bowieite–Kashinite series known as orogenic peridotite massives [54]. Enrichment in Pd relative to Pt is consistent with overall metasomatic/melt origin of the Cu-Ni mss.

Sulfide inclusions in Cr-spinel and in silicate minerals comprise a population of the e-type sulfides in Cpx-rich Spl lherzolite. Sulfide that is included in Cr-spinel (Figure 4c) has PGE characteristics and patterns similar to those observed for the e-type sulfides from Cpx-poor Spl lherzolite (Figure 7b). Sulfide phases from the inner part of the inclusion (Pn + Ccp) were characterized by the residual to metasomatic PGE signatures $((Pd/Ir)_N = 0.36–6.39)$ with fingerprints of secondary re-enrichment $([Pt/Pd]_N = 0.05–0.69)$. However, the outer part of the inclusion that is represented by chalcopyrite, displayed almost no signatures of metasomatic influence $((Pd/Ir)_N = 0.82$ and $[Pt/Pd]_N = 1.51)$. Chalcopyrite from the outer part of the inclusion displays an almost unfractionated PGE pattern with PGE concentrations being $\leq 10 \times$ CI chondrite (Figure 7c). Chalcopyrite of this type is directly adjacent to the chain of tiny sulfide blebs healing a former crack in the spinel grain (Figure 4c). This suggests that chalcopyrite originated as interstitial mss incorporated into spinel through the cracks (in liquid or semi liquid state) but not as a product of the mss break up. On the contrary, most e-type sulfides in silicates and i-type sulfides from the lherzolite matrix are characterized by the metasomatic/melt PGE signatures $((Pd/Ir)_N = 5.4–11.6)$ and show pronounced fingerprints of metasomatic Pd re-enrichment $([Pt/Pd]_N = 0.16–0.59)$. They display variably fractionated PGE patterns complicated by troughs at Ir and Pt and by sub- to suprachondritic PGE concentrations (Figure 7d). This evidently precipitated from silicate melts migrating through the lherzolite matrix as it follows the strong domination of the P-PGE over the I-PGE reflected in $((Pd/Ir)_N = 1.5–51.6)$. In this process, the i-type sulfides from Cpx-rich Spl lherzolits are similar to the i-type sulfides from Cpx-poor Spl lherzolites. However, two occurrences of the i-type sulfides represented by big multi-phase grains can be interpreted as carrying residual PGE signatures $((Pd/Ir)_N = 0.16–0.51)$ with no or with only subtle evidence of the metasomatic re-introduction of Pd $([Pt/Pd]_N = 0.57–1.33)$. These sulfides are characterized by very specific PGE patterns with a convex down I-PGE pattern followed by a deep trough at Pt (Figure 7a). Such distribution could be considered as typical for residual sulfides that are almost unaffected by enrichment processes (see Westner et al. [27]). Additionally, one group of the i-type sulfides was characterized by almost unfractionated PGE patterns $((Pd/Ir)_N = 1.28–3.02$; $[Pt/Pd]_N = 0.38–0.64)$ with PGE

concentrations of >10 × CI chondrite (Figure 7c). In this case, such sulfides are similar to chalcopyrite from their inclusion in spinel. Such characteristics could be typical of sulfides directly precipitated from the melt (see Westner et al. [27]).

Most analyzed sulfides in the Spl-Grt lherzolites were found inside kelyphite aggregates that replaced Grt. Since sulfides from kelyphite display obvious residual PGE signatures ((Pd/Ir)$_N$ = 0.09–0.32) and were virtually unaffected by metasomatic Pd re-introduction ([Pt/Pd]$_N$ = 0.55–1.05), it is likely that intrakelyphitic sulfides were initially included in garnet and therefore are associated with the e-type sulfides with typical residual PGE patterns (Figure 7a). The absence of evidence of metasomatic influence is interesting because during kelyphite formation, some melting occurred, which resulted in metasomatizing liquid [8]. Interstitial sulfides rarely observed in Spl-Grt lherzolites (Figure 5c,d) are enriched in the P-PGE relative to the I-PGE ((Pd/Ir)$_N$ = 1.2–44.6) and display fingerprints of metasomatic Pd re-introduction ([Pt/Pd]$_N$ = 0.06–0.45), which is overall typical for most i-type sulfides from all of the considered lherzolite types. Distribution of the PGE for the i-type sulfides is characterized by the two pattern styles, i.e., almost unfractionated PGE patterns with ≥10 × CI chondrite PGE concentrations (Figure 7d) and significantly fractionated PGE patterns often characterized by troughs at Ir and Pt and with PGE concentrations varying from just above chondritic to ≤100 × CI chondrite (Figure 7e).

In summary, most analyzed e-type sulfides maintain the residual PGE signatures and were only affected by metasomatic re-enrichment insignificantly, if at all. On the contrary, the i-type sulfides (with a few exceptions) display evidence of precipitation from the migrating silicate melts (melt-sulfides after Westner et al. [27]). Since sulfides with both residual and metasomatic PGE signatures coexist within a single xenolith sample, the PGE seem to be capable of effectively recording mantle processes related to mantle melting and intramantle melt migration (see Westner et al. [27]). Based on the observed PGE features, we interpret the e-type sulfides as residues of melting processes and the i-type sulfides as the crystallization products of sulfide-bearing (metasomatic) fluids/liquids (see Foley et al. [4], Kogarko et al. [9], Solovova et al. [11], Hughes et al. [40]).

Pyrite from silicate-carbonate patches in Spl-Grt lherzolites displays very low I-PGE content (down to complete absence of both Os and Ir), with most PGE represented by the P-PGE. This is consistent with metasomatic origin of these sulfides. Although the PGE patterns for pyrite are incomplete, there is some evidence of an unfractionated style of such patterns (Figure 7g). Co-violarite from metasomatic veinlets in both Cps-poor Spl and Spl-Grt lherzolites is characterized by unfractionated PGE patterns with suprachondritic concentrations of the elements at about 10 × CI chondrite (Figure 7g). This suggests a very simple m-sulfides origin that does not record histories of either depletion or re-enrichment.

4.4.2. Other Trace Elements

A number of studies that have been conducted on non-PGE trace elements so trace elements have shown that at upper mantle conditions, the extent of element partitioning into sulfide liquid depends on pressure, temperature, oxygen fugacity, and host rock composition [15,55–60]. Experimental studies have shown that at upper mantle conditions such as those suggested for the Jetty Peninsula lherzolite suite [2,4,12], partial melting depletes the elements in rocks that strongly partition into sulfide melts (P-PGE, Cu, S, Se, Te, Ni, Co, Ag, Pb, Bi, ±Sn, Sb, and As), whereas elements such as the I-PGE, Mo, Zn, Mn, and V tend to be retained in mantle residue [17,58,60–62]. The rest of the trace elements behave transitionally, either partitioning to sulfide melts or retaining in the residue. The behavior of most transitional elements depends especially strongly on the oxygen fugacity. Li and Audetat [58] and Steenstra et al. [60] showed that increasing fO_2 typically decreases trace element partitioning into sulfide liquid; therefore, increasing their retention in mantle residue.

We studied the behavior of chalcophile (Cu, Zn, Ga, Ge, As, Se, Ag, Cd, In, Sn, Sb, Te, Pb, and Bi) and a few siderophile (Mn, Ni, Co, and Mo) and lithophile (Ti and Cr) trace elements in different sulfide phases. The observed features were compared with

those acquired from experimental work for the system "mss–sulfide liquid–mafic silicate liquid" [58]. The experiments were performed at 15–30 kb and 1175–1300 °C, i.e., at the conditions close to those suggested for the Cpx-rich Spl and Spl-Grt lherzolites from East Antarctica [4].

Features of trace element distributions in the studied sulfides are depicted in CI chondrite-normalized spider-diagrams (Figure 8a–g). Distribution patterns of non-PGE trace elements look very similar for all sulfide types except for the m-type sulfides. Generally, siderophile elements and a part of the chalcophile elements display almost unfractionated patterns (often complicated, however, by peaks at Cu and Ag), with concentrations varying from chondritic to ~10 × CI chondrite. The right part of all spider diagrams in Figure 8 shows significant steady depletion in the chalcophile elements such as In, Sn, Ge, Ga, and often Zn and in lithophile Ti and Cr (down to ≥0.01 × CI chondrite).
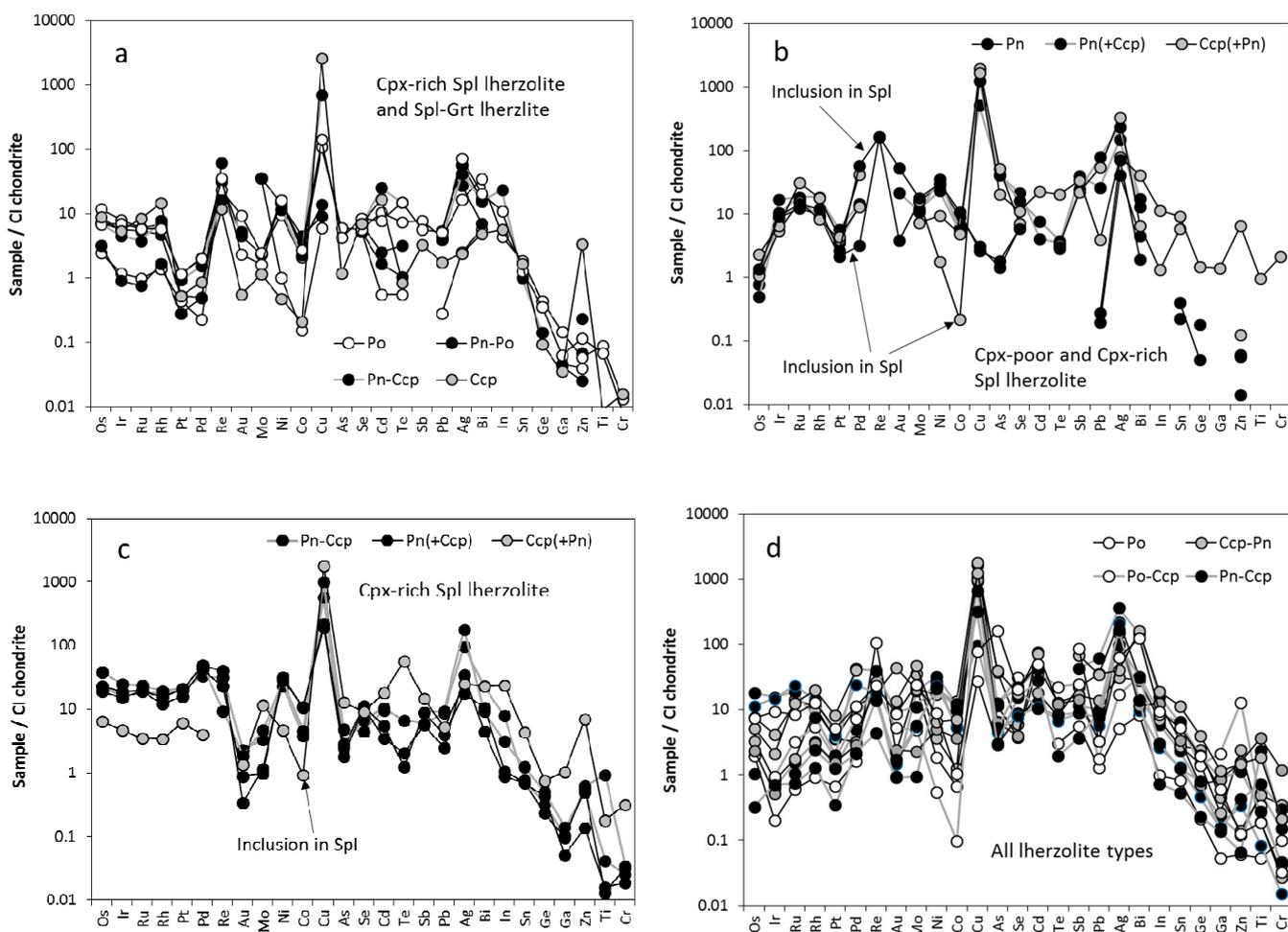
Figure 8. *Cont.*
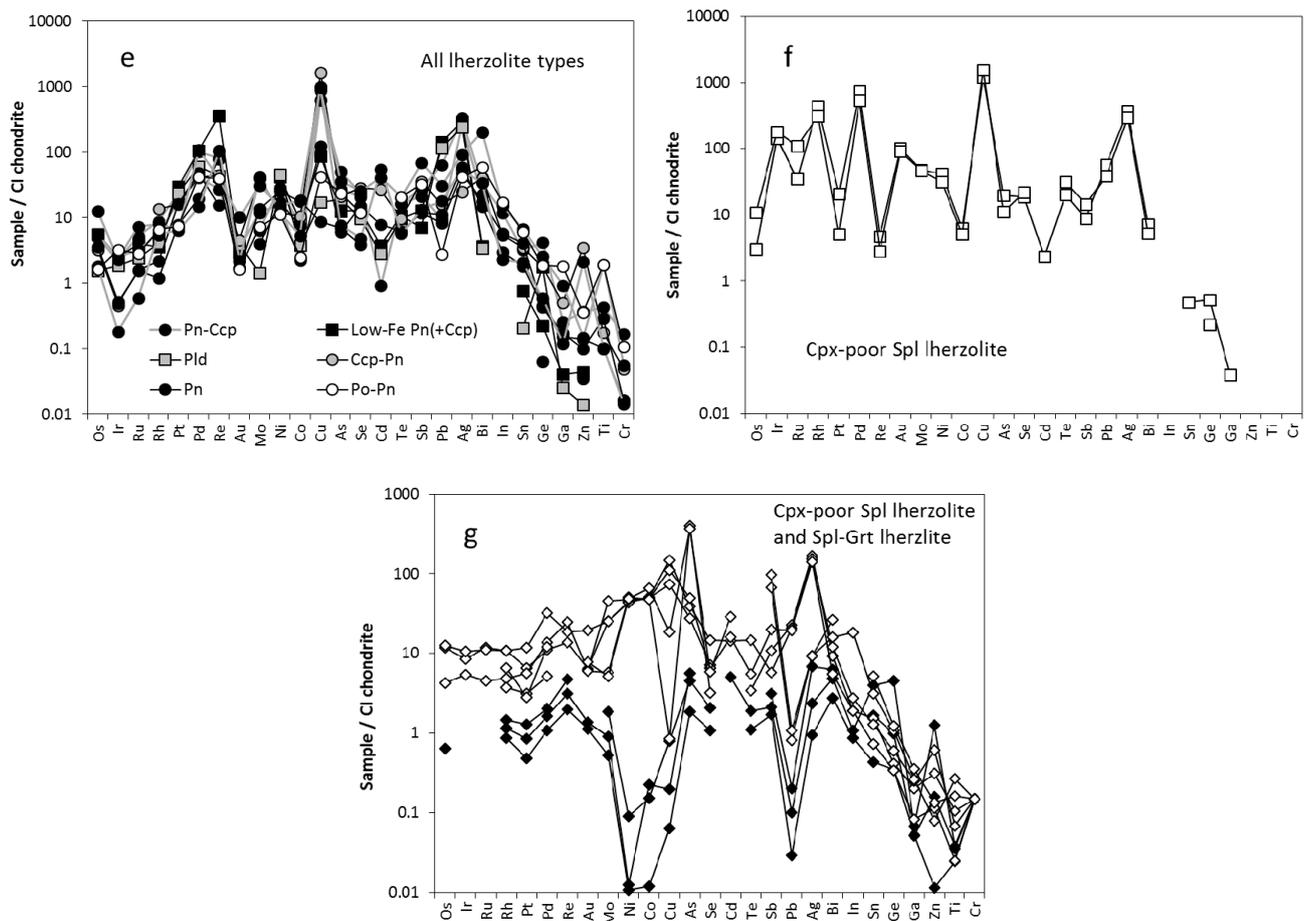
Figure 8. CI chondrite-normalized siderophile/chalcophile/lithophile element patterns for the studied sulfides (CI chondrite element concentrations are after Anders and Grevesse [41]). Diagrams are grouped according to the sulfide types identified on the basis of the PGE systematics (see Figure 7). (**a**) Unmetasomatized residual sulfides of the e- and i-types from Cpx-rich Spl lherzolites and Spl-Grt lherzolites. Peaks at Cu and Ag are observed for sulfides displaying mixed spectra, i.e., Pn-Ccp (see text for more details); (**b**) residual sulfides of the e-type in Cpx-poor Spl lherzolite and Cpx-rich Spl lherzolite. Peaks at Cu and Ag are observed for sulfides displaying mixed spectra (Pn-Ccp). Monomineral Pn does not display a peak at Cu, but it is still enriched in Ag; (**c**) melt-like (see Westner et al. [27]) sulfides of the i- and e-types that display unfractionated PGE patterns; all such melt-like sulfides display mixed spectra; (**d**) melt-like sulfides of the i- and e-types from all lherzolite types (most analyzed sulfides belong with this group) that display mixed but not significantly fractionated PGE patterns; (**e**) melt-like sulfides of the i-type that display the P-PGE as being significantly over the I-PGE in the PGE patterns. Sheer Pn and Pld do not display a peak at Cu, but they are still enriched in Ag; (**f**) Cu-Ni mss in Cpx-poor Spl lherzolite (no data on Ti and Cr are available); (**g**) partly incomplete patterns for m-type sulfides. Py displays generally unfractionated patterns complicated by troughs at Ni, Co, Cu, and Pb and subchondritic concentrations of Ti and Cr. Co-Vo is enriched in siderophile elements and is depleted in lithophile elements. Markers are as seen in Figure 7. Grey lines are for Pn-Ccp (see text for more details).

Base metal sulfides of the e-type are characterized by higher concentrations of both Ti and Cr than the BMS of the i-type sulfides (Table 5). This suggests "conservative" behavior of these lithophile elements during mantle melting and their preferable retention in the residue. Although Li and Audetat [58] did not include Ti and Cr in their experimental compositions, they showed that V (a proxy for Cr) would preferably be retained in the residue. An interesting observation was made for chalcopyrite from the sulfide inclusion in Cr-spinel (Figure 4c). Chalcopyrite developed along the edges of the inclusion displays strongly elevated concentrations of Cr (5659 ppm), whereas chalcopyrite from lamellae in the same inclusion does not show significant enrichment in Cr (823 ppm). Therefore, Cu-rich liquid incorporated into the Cr-spinel interior through the cracks and represented

now by massive chalcopyrite around the Pn-Ccp core seems to interact with the host Cr-spinel. Very low concentrations of Mn are typical for all sulfides from Cpx-poor Spl lherzolites: these are below the detection limits in the e-type sulfides and are 3–24 ppm for the i-type sulfides. A different picture was observed for Cpx-rich Spl lherzolites and Spl-Grt lherzolites. Here, the e-type sulfides contain more Mn than i-type sulfides. It therefore seems that at higher P-T conditions, Mn is preferably retained in the residue. This is consistent with experimental data suggesting that Mn behaves as a siderophile element and is retained in mantle residue. However, pentlandite from the sulfide inclusion in Cr-spinel (Cpx-rich Spl lherzolite) displays low concentrations of Mn (32–49 ppm) that are comparable to those in sulfides of the i-type. However, chalcopyrite that is developed along the marginal parts of the sulfide inclusion in Cr-spinel displays strongly elevated concentrations of Mn (2122 ppm). Once again, as in the case of Cr, chalcopyrite from the exsolution lamellae in the same inclusion is much poorer in Mn (497 ppm). This observation points once more to the interaction of Cu-rich sulfide material with the host mineral. Cobalt is a dominant siderophile trace element in most studied sulfide types. Because Co behaves coherently with Ni, pentlandite is expectedly the main concentrator of Co (>5000 ppm). There is no significant difference between the Co concentrations in pentlandite from sulfides of the e- and i-types (Table 5 and Table S1). Sulfides of both types were characterized by low Mo concentrations (mostly 1–10 $\times$ CI chondrite). For two analyses that have very high Mo concentrations in interstital pentlandite (1541–1561 ppm; Table 5 and Table S1), Mo forms zones of enrichment within a pentlandite body (Figure 9), probably due to the presence of molybdenite solid solution. Molybdenum is more concentrated in chalcopyrite from sulfides of the i-type than from sulfides of the e-type, whereas there are no differences in the concentration of the element in the pentlandite from sulfide of different types (Table 5 and Table S1). Thus, we suggest preferential partitioning of Mo to sulfide liquid relative to the residue. According to experimental studies, Mo mostly behaves as a transitional element with some tendencies to be retained in the residue. Therefore, the observed behavior of Mo in chalcopyrite could be due to certain P-T-fO$_2$ conditions that are typical for each lherzolite type.
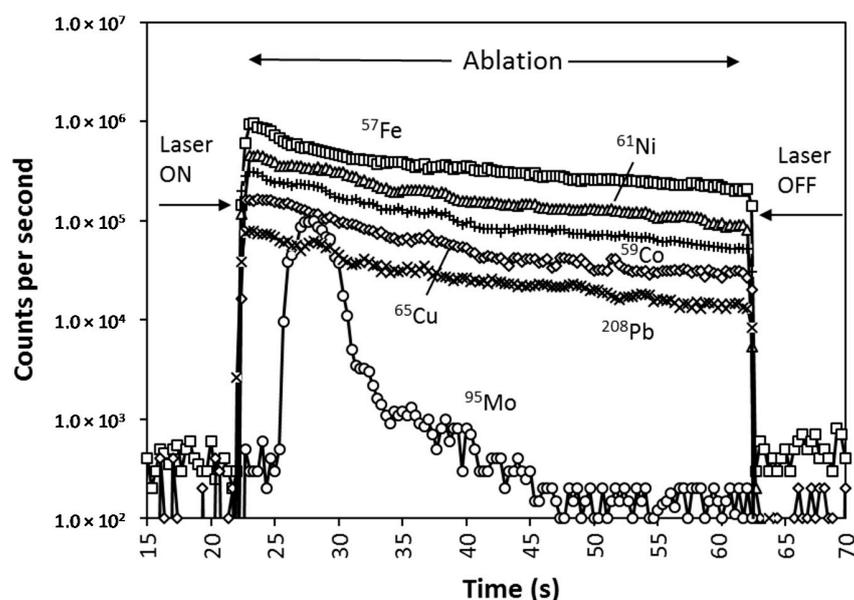

Figure 9. Representative time-resolved LA-ICP-MS depth profile for a sample U-1/4-3 (interstitial low-Fe Pn-Ccp from Cpx-poor Spl lherzolite) showing uneven Mo (isotope ^{95}Mo) distribution within the analyzed sulfide volume. From the left, the background count is 22 s (not shown completely) followed by 40 s of ablation time, which is integrated, and by 40 s of wash-out time (not shown completely). The laser beam encountered a Mo-rich inclusion at 26 s and had burnt through it at 34 s. A few selected isotopes with uniform distribution are shown for comparison.

Zinc does not show any preference in partitioning into a sulfide of any particular type, and Zn amounts are more dependent on the xenolith type. Concentrations of Zn are much lower in sulfides from Cpx-poor Spl lherzolite than in sulfides from Cpx-rich Spl lherzolite and Spl-Grt lherzolite. Since Cpx-poor Spl lherzolite was subjected to intensive melting and depletion [4], it seems that Zn was significantly removed from the rocks. The much higher concentrations of Zn in Cpx-rich Spl lherzolite and in Spl-Grt lherzolite could be due to metasomatic re-enrichment, which intensively affected these two lherzolite types [4]. Concentrations of Ga, Ge, and In are typically low in the studied sulfides (often below the detection limit), and no overall partitioning tendencies could be revealed at such a low concentration of the elements. However, chalcopyrite is richer in Ga than in other BMS, and concentrations of Ga are higher in the chalcopyrite from the e-type sulfides than those from the mineral of the i-type sulfides (Table 5 and Table S1). Since chalcopyrite is often a product of mss breakup and since Ga (like Cu) accumulates mostly in chalcopyrite, the amount of Ga in chalcopyrite would reflect that amount in the parental mss. Therefore, Ga would rather be retained in mantle residue during partial melting. Concentrations of Ge in the studied BMS are generally similar for the both e-type and i-type sulfides, with no partitioning preferences observed. Concentrations of Cd in pyrrhotite are higher than in pentlandite, and pyrrhotite from the e-type sulfides is richer in Cd (5.4–7.1 ppm) than the mineral from sulfides of the e-type (<1 ppm). It therefore seems that Cd, similar to Ga, would preferably be retained in the residue during partial melting. In spite of very low concentrations (Table 5 and Table S1), Sn and Sb show signatures of more preferable accumulation in e-type sulfides. Arsenic displays a slight tendency to partition more preferably into sulfide liquid that is more enriched in the i-type sulfides than in e-type sulfides although experimental data suggest that As would rather be retained in residue during partial melting. Selenium in the BSM does not show any partitioning preferences for any sulfide type. Silver displays much higher concentrations in e-type sulfides than in i-type sulfides (Table 5 and Table S1) in Cpx-poor Spl lherzolites, suggesting Ag being retained in the mantle residue during partial melting. For other lherzolites, however, there is no difference in the Ag concentrations in different sulfide types. Since the redox state does not significantly differ between the types of the studied lherzolites [4,30], it seems that the behavior of Ag would be rather sensitive to P-T conditions. The element would preferably be retained in residue at lower P-T but would partition to sulfide liquid at a higher P-T. Such behavior of Ag seems to be consistent with experimental data. Lead displays very similar behavior, suggesting that the partitioning of the element strongly depends on the P-T conditions. Although experimental studies show that while Pb is preferably retained in the residue (which is, in part, consistent with our observations for lower P-T), overall, the behavior of Pb is more complicated than that of Ag and requires more detailed study. Concentrations of Te are low but are higher than those of Ga, Ge, Cd, In, Sn, and Sb (Table 5 and Table S1). The element displays a pronounced tendency to preferably partition into the e-type sulfides and is retained in the residue during partial melting. Typically, low concentrations of Bi are characteristic for the both e-type and i-type sulfides. No tendencies in the distribution of the element were observed, but that was most likely due to low Bi concentration in most of the studied sulfides.

Interstitial Cu-Ni mss from Cpx-poor Spl lherzolite displays overall high concentrations of most trace elements (from <10 up to ~1000 × CI chondrite). The mss was not analyzed for Ti and Cr, but it displays a significant range of Mn concentrations (Table 5). Since Mn concentration directly correlates with the concentration of Fe, we suggest the presence of tiny Mn-Fe oxides within the mss matrix. Concentrations of Co (2560–3150 ppm) are lower in the Cu-Ni mss than those in pentlandite but are higher than in the BMS of the e- or i-types. This points to disequilibrium for the Cu-Ni mss that had not yet started to break up into the individual BMS. Concentrations of Mo are higher than in any other sulfide phase except for the i-type sulfides in Cpx-poor Spl lherzolite (Tables 5 and S1). These observations are consistent with the suggestion that at the P-T-fO_2 conditions typical for mantle rocks parental to the studied xenolith samples, Mo would rather partition to the

sulfide liquid than be retained in the residue. The Cu-Ni mss contains very low amounts of Zn (below the detection limit), which is generally consistent with our observations that the BMS from Cpx-poor Spl lherzolites are significantly depleted in Zn. This can also suggest that the Cu-Ni mss was locally generated and did not migrate from a remote mantle domain. The concentration of elements such as Ge, Ga, As, Cd, In, Sb, Sn, and Bi are very low in the Cu-Ni mss (often below the detection limit), suggesting either their preferential retention in the mantle residue during partial melting or their low overall concentration in the host rock. Cu-Ni mss contains very high amounts of the elements such as Se, Ag, Te, and Pb (Table 5), suggesting that they partition into sulfide liquid at certain P-T-fO$_2$ conditions. Trace element CI chondrite-normalized patterns (Figure 8f) are similar to those observed for the BMS (at higher trace element concentrations than for the Cu-Ni mss, however). If the Cu-Ni mss precipitated directly from the melt, then the primary trace element (other than the PGE) composition of the studied BMS (both e- and i-types) was significantly affected by the fractionation between sulfide phases due to the influence of melt fluids (as it can be judged from trace element chondrite-normalized patterns).

M-type sulfides typically contain moderate amounts of Ti and Cr with Co-violarite from Spl-Grt lherzolite displaying higher amounts of these elements (Table 6). On the contrary, Co-violarite from Cpx-poor Spl lherzolite contains the lowest amounts of Ti and Cr. Such differences suggest different Co-violarite origin conditions than those of the two xenolith types derived from different SCLM levels [4].

Interestingly enough, although Mn is supposed to behave coherently with Fe, both the highest and the lowest Mn amounts were measured in Fe-rich sulfides such as pyrite (Table 6). Among all sulfides, Co-violarite, by stoichiometry, is the richest in Co (up to 15 wt%), as it is a major element in this mineral. Pyrite contains only 1–113 ppm Co, which is consistent with Ni-poor nature of pyrite. Sulfides of the m-type typically contain Mo amounts that are similar to those of the i-type BMS. Concentrations of Zn are very variable in the m-type sulfides (Table 6), likely due to the very mobile and volatile nature of the element. Concentrations of Ga are low in all m-type sulfides, with the highest concentrations measured in Co-violarite (0.84–3.59 ppm). Sulfides of the m-type display the highest overall concentrations of volatile elements such as Ge and As among all of the studied sulfides (Table 6). This points to the potential participation of these two elements in the metasomatic re-enrichment of the BMS, probably at the crustal horizons. Among the m-type sulfides, pyrite contains the lowest amounts of Se (below 40 ppm), whereas Co-violarite displays elevated concentrations of Se (up to 273 ppm). Concentrations of Ag are low in pyrite and Co-violarite from Spl-Grt lherzolites (0.5–1.9 ppm), but they are high in Co-violarite from Cpx-poor Spl lherzolite (28–48 ppm). As shown for the BMS, Ag is very sensitive to P-T conditions. Therefore, different Ag concentrations suggest different conditions for the generation of metasomatic veinlets in Cpx-poor Spl lherzolites and in Spl-Grt lherzolites. Concentrations of Cd and Sb are generally low in most m-type sulfides except for Co-violarite from Cpx-poor lherzolite, which display non-typically high amounts of Cd (10–12 ppm) and Sb (1–8 ppm). Concentrations of In are often below or just slightly above the detection limit that is similar to the BMS from lherzolite matrix. Concentrations of Sn in m-type sulfides are generally similar to those observed in the BMS from the lherzolite matrix. Tellurium is unevenly distributed among the m-type sulfides, with concentrations varying from below the detection limit in some pyrite and Co-violarite from Spl-Grt lherzolite to 34 ppm in Co-volarite from Cpx-poor Spl lherzolite. Similarly, concentrations of Pb vary from being very low in pyrite and Co-violarite from Spl-Grt lherzolite (0.1–2.7 ppm) to being very high (>60 ppm) in Co-violarite from Cpx-poor Spl lherzolite. Such distributions of Te and Pb are supposed to be due to the P-T-(fO$_2$) conditions for the generation of the certain m-type sulfides. Bismuth is very poor in all m-type sulfides, with concentrations similar to those for the studied BMS. Co-violarite is enriched in siderophile elements and depleted in lithophile elements (Figure 8g). Trace element patterns for m-sulfides (Figure 8g) are different from those for BSM, suggesting a different origin of the m-type sulfides.

All things considered, we can say that unlike in the case of the PGE, only a few other trace elements (Ti, Cr, Cd, ±Mo) in the BMS from lherzolite xenoliths display pronounced preferences to either partition to the sulfide liquid or to be retained in the residue during partial melting. Observed partitioning is mostly consistent with experimental studies [58,60] and PGE features. Most analyzed trace elements (other than the PGE) however, display dual behavior, i.e., in some lherzolites they preferably partition to sulfide liquid, while in others they would be retained in the residue. Such dual behavior seems to depend strongly on the P-T-fO$_2$ conditions during partial melting, which is consistent with the features observed during the experimental runs [58,60]. Mostly similar trace element (other than the PGE) composition of the e-type and i-type sulfides accompanied by the dual behavior of most analyzed trace elements in the studied lherzolite xenoliths could point to the remobilization of interstitial sulfides and their aggressive influence on the sulfides enclosed in minerals. The presence of the chains of tiny sulfide droplets along existing or healed fractures in primary xenolith minerals (Figure 4b,c) might be the result of such remobilization. Unlike most other trace elements, the PGE show different concentrations in sulfides of the e- and i-types, likely due to much more conservative behavior of the PGE preserving their primary features from being affected by later metasomatic processes. Sulfides of the e-type display residual PGE characteristics, whereas the i-type sulfides mainly display fingerprints of the secondary metasomatic re-enrichment. The i-type sulfides carry residual PGE signatures in only a few cases. All of the conducted observations show that the suggestion of Dromgoole and Pasteris [19] regarding the lack of the compositional differences between the e- and i-type sulfides because of the incorporation of postmetasomatic S-bearing and CO$_2$-rich melts is close to reality. Such a lack of compositional differences was due to the later metasomatic re-enrichment of the e-type sulfides by the melts/fluids responsible for the generation of i-type sulfides. The few inconsistencies that exist between the experimental data and features observed in natural systems (lherzolite xenoliths) can be related to difficulties in precisely modeling the natural systems while preparing the experimental runs. Therefore, a complex approach including both the study of the natural systems and the experimental work at the upper mantle P-T-fO$_2$ conditions is necessary in order to have a comprehensive view of the features of trace element behavior in silicate-sulfide systems.

Among the m-type sulfides, the trace element characteristics of the Co-violarite from two different lherzolite types, i.e., from Cpx-poor Spl lherzolite (32601-9b) and Spl-Grt lherzolite (DN-4), provided an opportunity to compare features of the metasomatic fluids/melts affecting the SCLM rocks derived from different upper mantle levels. It is notable that Co-violarite from Cpx-poor Spl lherzolite has much higher concentrations of most trace elements (other than the PGE) than the mineral from Spl-Grt lherzolite (Table 6). While a sample (xenolith) of Cpx-poor Spl lherzolite was most likely trapped from the shallowest upper mantle horizons bordering the crust (as we can judge from the low ambient temperature (852 °C) and the composition of the xenolith), a sample of Spl-Grt lherzolite was trapped from much deeper upper mantle horizons (T = 1125 °C; P = 21.5 kb; [4]). Since all of the studied xenoliths were collected from the same magmatic body and because they were delivered to the surface relatively quickly, it is unlikely that there was much variability in the interaction of the individual xenoliths with the transporting melt. Since the Cpx-poor Spl lherzolite xenolith 32601-9b might have been trapped from the uppermost mantle horizons bordering the lower crust, the influence of crustal fluids that are rich in elements such as Te, Pb, Ag, Se, and Zn might have been strong at those horizons. On the other hand, the metasomatic alteration experienced by the Spl-Grt lherzolite xenolith DN-4 might have been due to the migration of the intramantle fluids (silicate melt-related?) which were relatively depleted in "crustal" trace elements and instead enriched in elements such as As, Ge, Sn, and Sb.

5. Conclusions

The studied sulfides from the Jetty Peninsula SCLM lherzolite xenoliths are developed as inclusions in rock-forming minerals, interstitial grains between such minerals, tiny blebs along the fracture surfaces in primary minerals, and individuals in carbonate-silicate patches and metasomatic veinlets cross-cutting the lherzolite primary mineral assemblages. Sulfide modal abundance in the xenoliths is Cpx-poor lherzolites $\leq$ Spl-Grt lherzolites << Cpx-rich lherzolites, with major mineral assemblages of pentlandite + chalcopyrite $\pm$ pyrrhotite. Minor and rare sulfides are polydymite, millerite, violarite, siegenite, and the mss. A portion of the primary immiscible sulfide liquid formed during the partial melting of mantle material was trapped in the solid–liquid residuum represented by the lherzolite and eventually ended up as the BMS. The multiphase sulfide assemblages in the lherzolite xenolith matrix are not of primary mantle origin, but a product of subsolidus re-equilibration of the primary high-temperature mss. The major-element composition of the sulfide assemblages indicates that subsolidus low-temperature equilibration was incomplete and likely stopped at temperatures $\leq$300 °C.

More conservative PGE preserve primary features showing that e-type sulfides represent either residues from the melting processes or resulted from the remobilization of sulfide liquid incorporated in the host minerals along the cracks. The i-type sulfides are crystallization products of intramantle sulfide-bearing fluids/melts. The i-type sulfides very rarely display residual PGE signatures. Only a few non-PGE trace elements record residual characteristics in e-type sulfides. The most mobile trace elements that partitioned into interstitial sulfide liquid could metasomatically re-enrich residual sulfides of the e-type by overprinting their residual signatures. Such dual behavior of the trace elements seems to strongly depend on P-T-fO$_2$ conditions during and after partial melting. The i-type sulfides record the trace element characteristics of crystallization from the intramantle sulfide-bearing melts/fluids. Sulfide-bearing metasomatic veinlets and silicate-carbonate patches might have resulted from low-temperature metasomatism at the basis of the Earth's crust and localized at the intramantle metasomatism due to percolating immiscible sulfide-carbonate-silicate fluids/melts. A complex approach including both a study of the natural systems and experimental work at the upper mantle P-T-fO$_2$ condition is necessary in order to have a comprehensive view of trace element behavior in silicate-sulfide systems.

References

1. Laiba, A.A.; Andronikov, A.V.; Egorov, L.S.; Fedorov, L.V. Stock-like and dyke bodies of alakaline-ultramafic composition in Jetty Peninsula (Prince Charles Mountains, East Antarctica). In *Geological and Geophysical Investigations in Antarctica*; Ivanov, V.L., Grikurov, G.E., Eds.; PGO "Sevmorgeologia": Leningrad, Russia, 1987; pp. 35–47. (In Russian)

2. Andronikov, A.V. Spinel-garnet lherzolite nodules from alkaline-ultrabasic rocks of Jetty Peninsula (East Antarctica). *Antarctic Sci.* **1990**, *2*, 321–330. [CrossRef]

3. Andronikov, A.V. The first study of upper mantle inclusions from the Prince Charles Mountains, East Antarctica. In *Recent Progress in Antarctic Earth Science*; Yoshida, Y., Kaminuma, K., Shiraishi, K., Eds.; Terrapub: Tokyo, Japan, 1992; pp. 163–171.

4. Foley, S.F.; Andronikov, A.V.; Jacob, D.E.; Melzer, S. Evidence from Antarctic mantle peridotite xenoliths for changes in mineralogy, geochemistry and geothermal gradients beneath a developing rift. *Geochim. Cosmochim. Acta* **2006**, *70*, 3096–3120. [CrossRef]

5. Foley, S.F.; Andronikov, A.V.; Halpin, J.A.; Daczko, N.R.; Jacob, D.E. Mantle rocks in East Antarctica. *Geol. Soc. London Mem.* **2021**, *56*. [CrossRef]

6. Mikhalsky, E.; Andronikov, A.; Leitchenkov, G.; Belyatsky, B. The age of the Earth's crust in the Northern Prince Charles Mountains (East Antarctica) as evidenced by zircon xenocrysts from Cretaceous alkaline-ultramafic rocks. *Lithos* **2020**, *368–369*. [CrossRef]

7. Andronikov, A.V.; Beliatsky, B.V. Implication of Sm-Nd isotopic systematics to the events recorded in the mantle-derived xenoliths from the Jetty Peninsula, East Antarctica. *Terra Antart.* **1995**, *2*, 103–110.

8. Andronikov, A.V. Varying glass compositions in deep-seated inclusions from alkaline-ultamafic rocks of Jetty Peninsula (East Antarctica): Evidence for mantle metasomatism. In *The Antarctic Region: Geological Evolution and Processes*; Ricci, C.A., Ed.; Terra Antartica Publication: Siena, Italy, 1997; pp. 901–910.

9. Kogarko, L.N.; Kurat, G.; Ntaflos, T. Henrymeyerite in the metasomatized upper mantle of Eastern Antarctica. *Canad. Mineral.* **2007**, *45*, 497–501. [CrossRef]

10. Buikin, A.I.; Solovova, I.P.; Verchovsky, A.B.; Kogarko, L.N.; Averin, A.A. PVT parameters of fluid inclusions and the C, O, N, and Ar isotopic composition in a garnet lherzolite xenolith from the Oasis Jetty, East Antarctica. *Geochem. Intl.* **2014**, *52*, 805–821. [CrossRef]

11. Solovova, I.P.; Kogarko, L.N.; Averin, A.A. Conditions of sulphide formation in the metasomatized mantle beneath East Antarctica. *Petrology* **2015**, *23*, 519–542. [CrossRef]

12. Beliatsky, B.V.; Andronikov, A.V. Deep-seated lherzolite inclusions from alkaline-ultramafic rocks in Jetty Peninsula: The mineral and chemical composition, P-T conditions and Sr-Nd isotope systematic. In *Scientific Results of Russian Geological and Geophysical Researches in Antarctica 2*; Mikhalsky, E.V., Laiba, A.A., Eds.; VNIIOkeangeologia: St. Petersburg, Russia, 2009; pp. 89–109, (In Russian with English afterword).

13. Shindo, K.; Komuro, K.; Hayashi, K. Sulfide minerals in mantle xenoliths from the Kurose reef, Fukuoka Prefecture, Japan. *J. Mineral. Petrol. Sci.* **2009**, *104*, 182–187. [CrossRef]

14. Vaughan, D.J.; Corkhill, C.L. Mineralogy of sulfides. *Elements* **2017**, *13*, 81–87. [CrossRef]

15. Kiseeva, E.S.; Wood, B.J. The effects of composition and temperature on chalcophile and lithophile element partitioning into magmatic sulphides. *Earth Planet. Sci. Lett.* **2015**, *424*, 280–294. [CrossRef]

16. Kiseeva, E.S.; Fonseca, R.O.C.; Smythe, D.J. Chalcophile elements and sulfides in the upper mantle. *Elements* **2017**, *13*, 111–116. [CrossRef]

17. Alard, O.; Griffin, W.L.; Lorand, J.-P.; Jackson, S.E.; O'Reilly, S.Y. Non-chondritic distribution of the highly siderophile elements in mantle sulfides. *Nature* **2000**, *407*, 891–894. [CrossRef] [PubMed]

18. Griffin, W.L.; Graham, S.; O'Reilly, S.Y.; Pearson, N.J. Lithosphere Evolution beneath the Kaapvaal Craton: Re-Os systematics of sulfides in mantle-derived peridotites. *Chem. Geol.* **2004**, *208*, 89–118. [CrossRef]

19. Dromgoole, E.L.; Pasteris, J.D. Interpretation of the sulfide assemblages in a suite of xenoliths from Kilbourne Hole, New Mexico. *Geol. Soc. Amer. Spec. Paper* **1987**, *215*, 25–46.

20. Szabo, C.; Bodnar, R.J. Chemistry and origin of mantle sulfides in spinel peridotite xenoliths from alkaline basaltic lavas, Nógrád Gömör Volcanic Field, northern Hungary and southern Slovakia. *Geochim. Cosmochim. Acata* **1995**, *59*, 3917–3927. [CrossRef]

21. Guo, J.; Griffin, W.L.; O'Reilly, S.Y. Geochemistry and origin of sulphide minerals in mantle xenoliths: Qilin, Southeastern China. *J. Petrol.* **1999**, *40*, 1125–1149. [CrossRef]

22. Lorand, J.P.; Gregoire, M. Petrogenesis of base metal sulfide assemblages of some peridotites from the Kaapvaal Craton (South Africa). *Contrib. Mineral. Petrol.* **2006**, *151*, 521–538. [CrossRef]

23. O'Reilly, S.Y.; Griffin, W.L. Imaging global chemical and thermal heterogeneity in the subcontinental lithospheric mantle with garnets and xenoliths: Geophysical implications. *Tectonophysics* **2006**, *416*, 289–309. [CrossRef]

24. Sen, I.S.; Bizimis, M.; Sen, G. Geochemistry of sulfides in Hawaiian garnet pyroxenite xenoliths: Implications for highly siderophile elements in the oceanic mantle. *Chem. Geol.* **2010**, *273*, 180–192. [CrossRef]

25. Delpech, G.; Lorand, J.-P.; Gregoire, M.; Cottin, J.-Y.; O'Reilly, S.Y. In-situ geochemistry of sulfides in highly metasomatized mantle xenoliths from Kerguelen, southern Indian Ocean. *Lithos* **2012**, *154*, 296–314. [CrossRef]

26. Lorand, J.P.; Luguet, A.; Alard, O. Platinum-group element systematics and petrogenetic processes of the continental mantle: A review. *Lithos* **2013**, *164*, 2–21. [CrossRef]

27. Westner, K.J.; Beier, C.; Klemd, R.; Osbahr, I.; Brooks, N. In situ chalcophile and siderophile element behavior in sulfides from Moroccan Middle Atlas spinel peridotite xenoliths during metasomatism and weathering. *Minerals* **2019**, *9*, 276. [CrossRef]

28. Andronikov, A.V.; Egorov, L.S. Mesozoic alkaline-ultramafic magmatism of Jetty Peninsula. In *Gondwana Eight: Assembly, Evolution and Dispersal*; Findlay, R.H., Unrug, R., Banks, M.R., Veevers, J.J., Eds.; Balkema; Brookfield: Rotterdam, The Netherlands, 1993; pp. 547–557.

29. Foley, S.F.; Andronikov, A.V.; Melzer, S. Petrology of ultramafic lamprophyres from the Beaver Lake area of Eastern Antarctica and their relation to the breakup of the Gondwanaland. *Mineral. Petrol.* **2002**, *74*, 361–384. [CrossRef]

30. Andronikov, A.V.; Sheraton, J.W. The redox state of the lithospheric upper mantle beneath the East Antarctic Shield. *Terra Antarct.* **1996**, *3*, 39–48.

31. van Achterbergh, E.; Ryan, C.G.; Jackson, S.E.; Griffin, W.L. Data reduction software for LA-ICP-MS. In *Laser-Ablation-ICPMS in the Earth Sciences: Principles and Applications*; Sylvester, P., Ed.; Mineral. Assoc. Canada Short Course Series; Mineralogical Association of Canada: Quebec City, QC, Canada, 2001; Volume 29, pp. 239–243.

32. Griffin, W.L.; Powell, W.J.; Pearson, N.J.; O'Reilly, S.Y. GLITTER: Data reduction software for laser ablation ICP-MS. In *Laser Ablation ICP–MS in the Earth Sciences: Current Practices and Outstanding Issues*; Sylvester, P., Ed.; Mineralogical Association of Canada Short Course Series; Mineralogical Association of Canada: Quebec City, QC, Canada, 2008; Volume 40, pp. 308–311.

33. Wilson, S.A.; Koenig, A.E.; Ridley, W.I. Development of sulfide calibration standards for the laser ablation inductively-coupled plasma mass spectrometry. *J. Anal. Atom. Spectrom.* **2002**, *17*, 406–409. [CrossRef]

34. Savard, D.; Bouchard-Boivin, B.; Barnes, S.-J.; Garbe-Schönberg, D. UQAC-FeS: A new series of base metal sulfide quality control reference material for LA-ICP-MS analysis. In Proceedings of the 10th International Conference on the Analysis of Geological and Environmental Materials, Sydney, Australia, 8–13 July 2018.

35. Duran, C.J.; Dube-Loubert, H.; Page, P.; Barnes, S.J.; Roy, M.; Savard, D.; Cave, B.J.; Arguin, J.-P.; Mansur, E.T. Applications of trace element chemistry of pyrite and chalcopyrite in glacial sediments to mineral exploration targeting: Example from the Churchill Province, northern Quebec, Canada. *J. Geochem. Explor.* **2019**, *196*, 105–130. [CrossRef]

36. Mathieu, L.; Racicot, D. Petrogenetic Study of the Multiphase Chibougamau Pluton: Archaean Magmas Associated with Cu–Au Magmato-Hydrothermal Systems. *Minerals* **2019**, *9*, 174. [CrossRef]

37. Ballhaus, C.; Sylvester, P. 2000. Noble metal enrichment processes in the Merensky Reef, Bushveld Complex. *J. Petrol.* **2000**, *41*, 546–561. [CrossRef]

38. Cook, N.; Ciobanu, C.L.; George, L.; Zhu, Z.-Y.; Wade, B.; Ehrig, K. Trace Element Analysis of Minerals in Magmatic-Hydrothermal Ores by Laser Ablation Inductively-Coupled Plasma Mass Spectrometry: Approaches and Opportunities. *Minerals* **2016**, *6*, 111. [CrossRef]

39. Pettke, T. Analytical protocol for element concentration and isotope ratio measurement in fluid inclusions by LA–(MC–)ICP–MS. In *Laser Ablation–ICP–MS in the Earth Sciences*; Sylvester, P., Ed.; Mineralogical Association of Canada Short Course; Mineralogical Association of Canada: Quebec City, QC, Canada, 2008; Volume 40, pp. 189–217.

40. Hughes, H.S.R.; McDonald, I.; Faithfull, J.W.; Upton, B.G.J.; Loocke, M. Cobalt and precious metals in sulphides of peridotite xenoliths and inferences concerning their ditribution according to geodynamic environment: A case study from the Scottish lithospheric mantle. *Lithos* **2016**, *240–243*, 202–227. [CrossRef]

41. Anders, E.; Grevesse, N. Abundances of the elements: Meteoritic and solar. *Geochim. Cosmochim. Acta* **1989**, *53*, 197–214. [CrossRef]

42. Mitchell, R.H.; Keays, R.R. Abundance and distribution of gold, palladium and iridium in some spinel and garnet lherzolites: Implications for the nature and origin of precious metal-rich intergranular components in the upper mantle. *Geochim. Cosmochim. Acta* **1981**, *45*, 2425–2445. [CrossRef]

43. Ebel, D.S.; Naldrett, A.J. Fractional crystallization of sulfide ore liquids at high temperature. *Econom. Geol.* **1996**, *91*, 607–621. [CrossRef]

44. Ebel, D.S.; Naldrett, A.J. Crystallization of sulfide liquids and interpretation of ore composition. *Canad. J. Earth Sci.* **1997**, *34*, 352–365. [CrossRef]

45. Mungall, J.A. Crystallization of magmatic sulfides: An empirical model and application to Sudbury ores. *Geochim. Cosmochim. Acta* **2007**, *71*, 2809–2819. [CrossRef]

46. Nkoumbou, C.; Villieras, F.; Barbey, P.; Ngoune, C.-Y.; Joussemet, R.; Diot, F.; Njopwouo, D.; Yvon, J. Ni-Co sulphide segregation in the Mamb pyroxenite intrusion, Cameroon. *Comptes Rendus Geosci.* **2009**, *341*, 517–525. [CrossRef]

47. Kitakaze, A.; Komatsu, R. Phase relations of some sulfide systems-(5). Especially Fe-Ni-S system. In *Memoirs of the Faculty of Engenieering, Yamaguchi University*; Yamaguchi University: Yamaguchi, Japan, 2020; Volume 70, pp. 1–22.

48. Kullerud, G.; Yund, R.A.; Moh, G. Phase relation in the Cu-Fe-S and Cu-Ni-S systems. *Econ. Geol.Monogr.* **1969**, *4*, 323–343.

49. Kelly, D.P.; Vaughan, D.J. Pyrrhotine-pentlandite ore textures: A mechanistic approach. *Mineral. Mag.* **1983**, *47*, 453–463. [CrossRef]

50. Wang, H.; Pring, A.; Ngothai, Y.; O'Neil, B. A low-temperature kinetic study of the exsolution of pentlandite from the monosulfide solid solution using a refined Avrami method. *Geochim. Cosmochim. Acta* **2005**, *69*, 415–425. [CrossRef]

51. Bishop, F.C.; Smith, J.V.; Dawson, J.B. Pentlandite-magnetite intergrowth in the De Beers spinel lherzolite: Review of sulfide in nodules. *Phys. Chem. Earth* **1975**, *9*, 323–337. [CrossRef]

52. Raghavan, V. Phase diagram evaluation: Section II. Fe-Ni-S (Iron-Nickol-Sulfur). *J. Phase Equilibria Diffus.* **2004**, *25*, 373–381. [CrossRef]

53. Krymsky, R.S.; Antonov, A.V.; Belyatsky, B.V.; Sushchevskaya, N.M.; Sergeev, S.A. The age and the evolution of the lithospheric mantle in the East Antarctic Craton: Osmium isotope composition and the distribution of the platinum group elements in spinel lherzolite nodules. *Doklady Earth Sci.* **2019**, *485*, 444–449. [CrossRef]

54. Zaccarini, F.; Pushkarev, E.; Garuti, G.; Bindi, L. Multi-Analytical Characterization of Minerals of the Bowieite–Kashinite Series from the Svetly Bor Complex, Urals, Russia, and Comparison with Worldwide Occurrences. *Canad. Mineral.* **2016**, *54*, 461–473. [CrossRef]

55. Kiseeva, E.S.; Wood, B.J. A simple model for chalcopyrite element partitioning between sulphide and silicate liquids with geochemical applications. *Earth Planet. Sci. Lett.* **2013**, *383*, 68–81. [CrossRef]

56. Brenan, J.M. Re-Os fractionation by sulfide melt-silicate melt partitioning: A new spin. *Chem. Geol.* **2008**, *248*, 140–165. [CrossRef]

57. Brenan, J.M. Se-Te fractionation by sulfide-silicate melt partitioning: Implications for the composition of mantle-derived magmas and their melting residues. *Earth Planet. Sci. Lett.* **2015**, *299*, 328–338. [CrossRef]

58. Li, Y.; Audetat, A. Partitioning of V, Mn, Co, Ni, Cu, Zn, As, Mo, Ag, Sn, Sb, W, Au, Pb and Bi between sulfide phases and hydrous basanite melt at upper mantle conditions. *Earth Planet. Sci. Lett.* **2012**, *355–356*, 327–340. [CrossRef]

59. Greaney, A.T.; Rudnick, R.L.; Helz, R.T.; Gaschnig, R.M.; Piccoli, P.M.; Ash, R.D. The behavior of chalcophile elements during magmatic differentiation as observed in Kilauea Iki lava lake, Hawaii. *Geochim. Cosmochim. Acta* **2017**, *210*, 71–96. [CrossRef]

60. Steenstra, E.S.; Trautner, V.T.; Berndt, J.; Klemme, S.; van Westrenen, W. Trace element partitioning between sulfide-, metal-, and silicate melts at highly reduced conditions: Insights into the distribution of volatile elements during core formation in reduced bodies. *Icarus* **2020**, *335*, 113408. [CrossRef]

61. Ballhaus, C.; Tredoux, M.; Späth, A. Phase relations in the Fe–Ni–Cu–PGE–S system at magmatic temperature and application to massive sulphide ores of the Sudbury igneous complex. *J. Petrol.* **2001**, *42*, 1911–1926. [CrossRef]

62. Lorand, J.P.; Luguet, A.; Alard, O. Platinum-group elements: A new set of key tracers for the earth's interior. *Elements* **2008**, *4*, 247–252. [CrossRef]